US 20170189276A1

(19) **United States**

(12) **Patent Application Publication** (10) **Pub. No.: US 2017/0189276 A1**

Wilkinson et al. (43) **Pub. Date: Jul. 6, 2017**

(54) **METHOD FOR CREATING A MINERAL TRIOXIDE AGGREGATE MATERIAL WITH IMPROVED BIOLOGICAL EFFECTS**

(71) Applicant: **DENTSPLY SIRONA, Inc.**, York, PA (US)

(72) Inventors: **Kevin Wilkinson**, Bixby, OK (US); **Geoffrey Ndungu**, Tulsa, OK (US)

(73) Assignee: **DENTSPLY SIRONA, Inc.**, York, PA (US)

(21) Appl. No.: **15/140,586**

(22) Filed: **Apr. 28, 2016**

Related U.S. Application Data

(60) Provisional application No. 62/154,282, filed on Apr. 29, 2015.

Publication Classification

(51) **Int. Cl.**

A61K 6/06	(2006.01)
C23C 14/22	(2006.01)
B28B 11/24	(2006.01)
C04B 28/04	(2006.01)
B28B 1/14	(2006.01)

(52) **U.S. Cl.**

CPC ***A61K 6/0606*** (2013.01); ***C04B 28/04*** (2013.01); ***B28B 1/14*** (2013.01); ***B28B 11/24*** (2013.01); ***C23C 14/22*** (2013.01); *C04B 2103/0067* (2013.01)

(57) **ABSTRACT**

A dental device is improved in its ability to produce hydroxyl apatite by having a layer of mineral trioxide aggregate (MTA) deposited thereon. A tile of MTA is prepared, heat treated and sintered to produce a micronized tile of MTA that can then be deposited by physical vapor depositions, hot isostatic pressing, molding or other conventional technique.

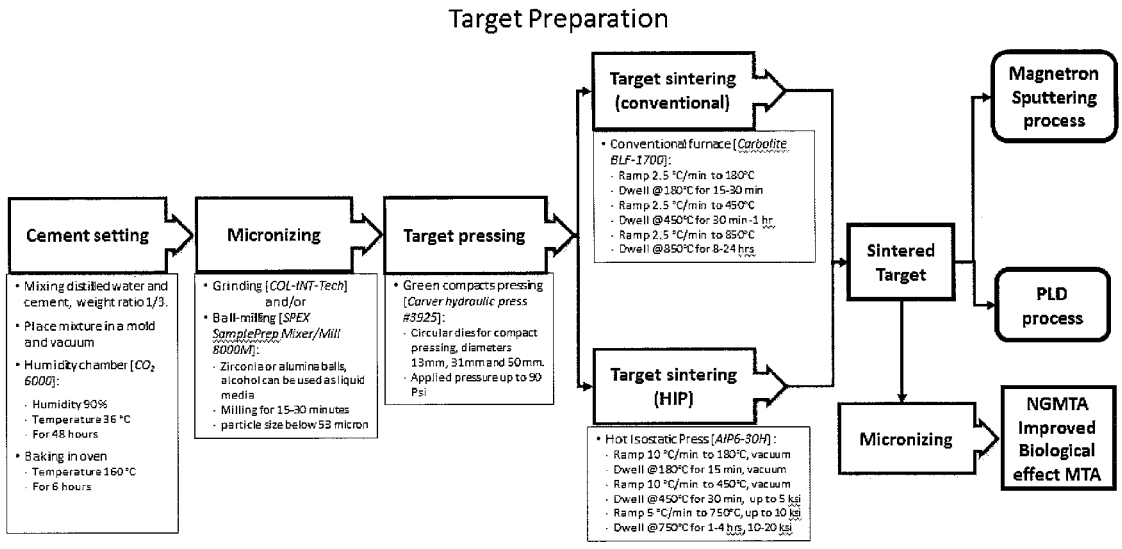

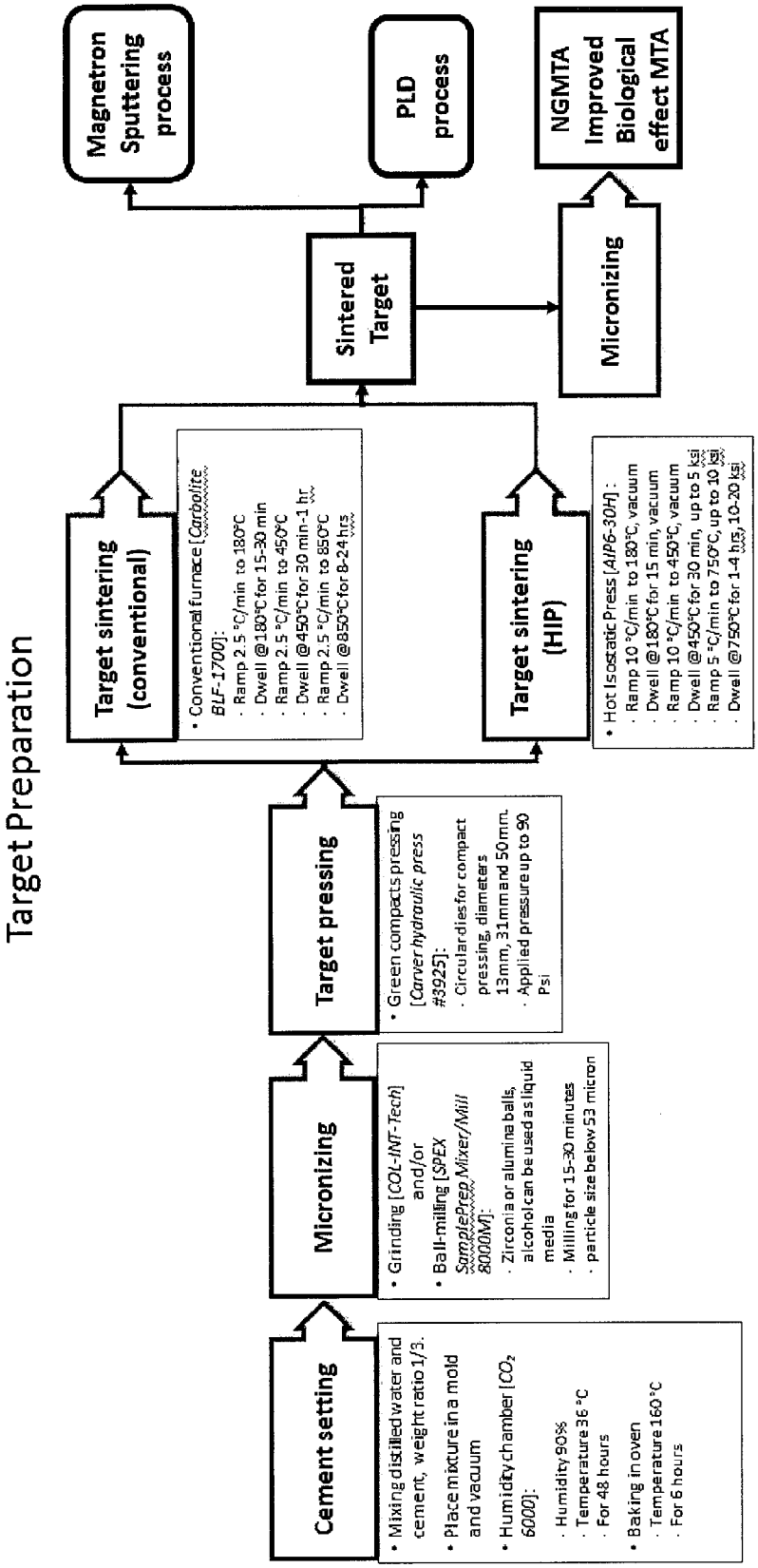

Figure 1. Target preparation process flow chart.

- Ball-Milling (15 Minutes)
- Pressing (1.5 ton, Diameter=13mm, Pressure=111 MPa)
- Sintering 850°C

Sample set	Process parameters		Weight lost (%)		Volume lost (%)		Density (g/cm3)	
	Heating rate (°C/min)	Dwell time (hours)	Mean	STD	Mean	STD	Mean	STD
Set 3:1							2.07	0.071
Set 1	10	8	14.8	0.013	15.3	0.29	2.21	0.183
Set 2	2	2	14.6	0.039	13.3	0.37	2.23	0.107
Set 3	10	2	14.0	0.081	10.1	1.83	2.15	0.118
Set 4	2	8	15.1	0.036	15.6	0.42	2.35	0.355

Figure 2A: Data for Effect of Sintering parameters on target density.

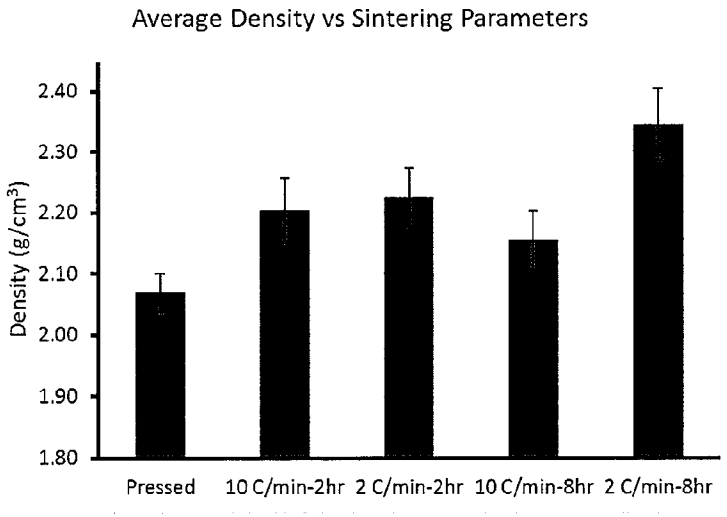

- Lower heating rate and longer dwell time leads to higher density.
- There was no significant changes in elemental composition due to sintering.
- It was also shown that heat treated WPC produces 10 times more HA when immersed in SBF.

Figure 2B. Chart of the Effect of sintering parameters on targets density.

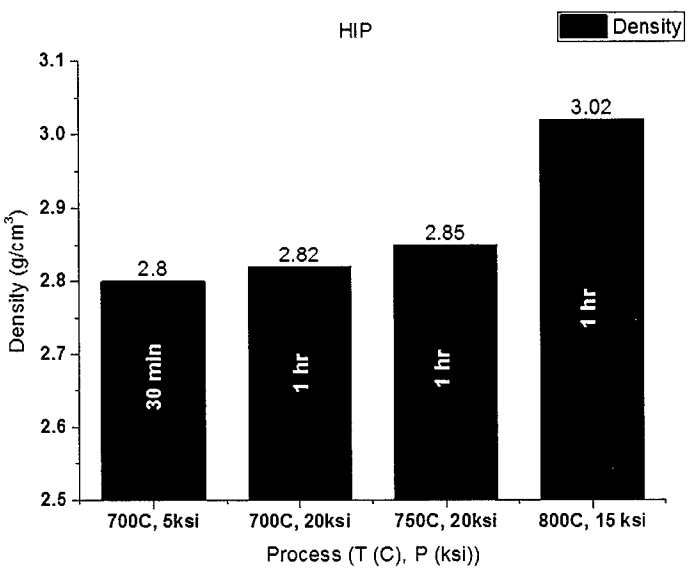

Figure 3A: Effect of HIP parameters on target density chart.

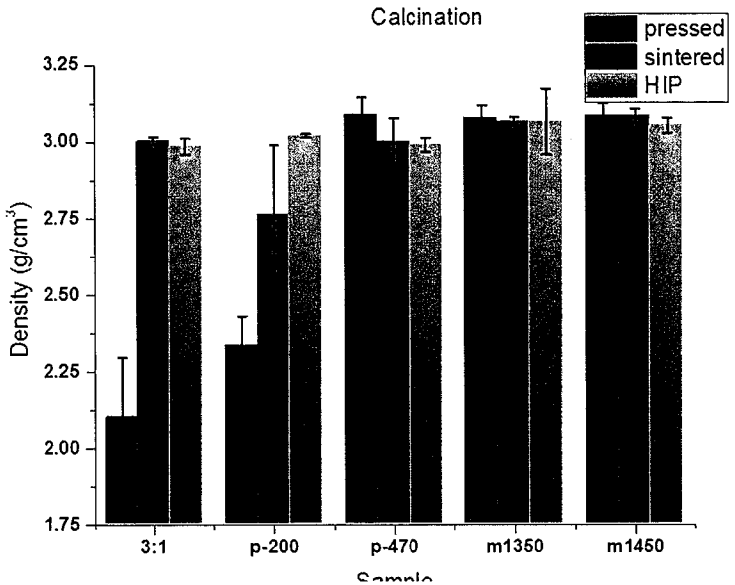

Figure 3B: Effect of pre-calcination on target density chart.

- The green compact preparation procedure (additional ball-milling, pressing in carver press at 90-120 MPa) has the highest impact on density of sintered ceramics (samples h1-h7, ρ =1.8 -2.4 g/cm^3 vs ρ >2.6 g/cm^3)
- HIP: Process temperature has higher impact on density than pressure.
- Calcination (heat treatment of powder before ball-milling and pressing in order to remove CO_2 and water) at temperatures above 450 °C help to achieve similar densities for HIP and conventional sintering.

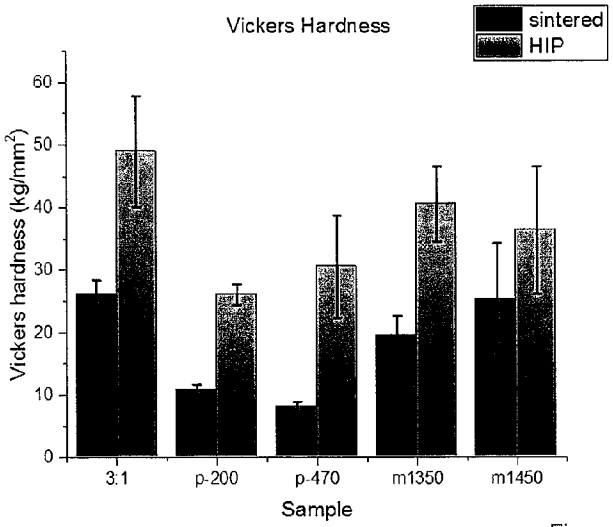

Figure 4A: Effect of sintering parameters on mechanical properties on target chart.

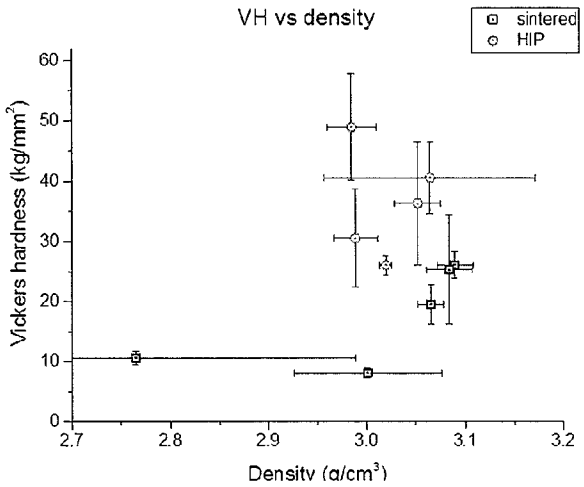

Figure 4B: Effect of sintering parameters on mechanical properties on target chart.

- There is a significant difference in Vickers hardness (VH) between conventional and HIP sintering samples. The VH of HIP-sintered samples is 30-50% higher.
- However, the calcination before sintering doesn't improve hardness of sintered cement (both conventional and HIP-sintered).

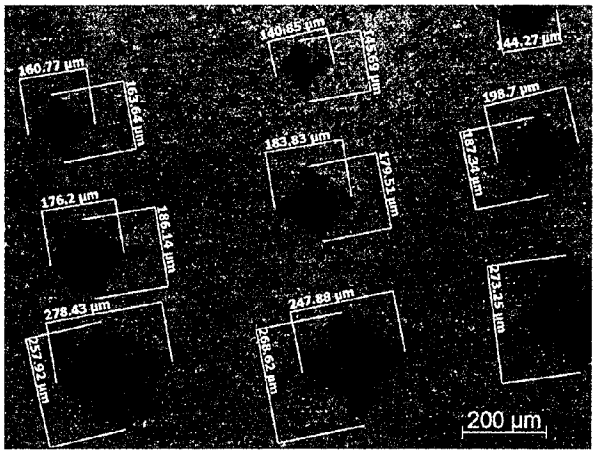

Figure 4C. Photo of samples taken to show the Effect of sintering parameters on mechanical properties on target

Figure 5A: Chart on the Effects of elemental composition of a pre-sintered target.

Figure 5B: Chart on the Effects of elemental composition of a conventional sintered target.

Figure 5C: Chart on the Effects of elemental composition of a HIP sintered target.

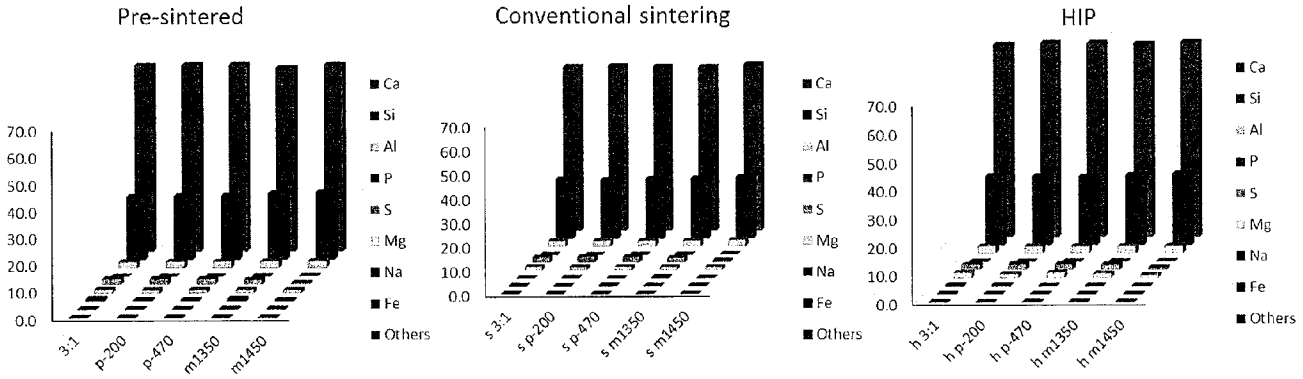

	Ca	Si	Al	P	S	Mg	Na	Fe	Others
3:1	68.9	23.4	2.4	0.1	2.2	1.4	1.0	0.4	0.3
p-200	69.0	23.6	2.5	0.0	2.3	1.2	0.6	0.4	0.3
p-470	69.0	23.6	2.5	0.1	2.2	1.3	0.6	0.4	0.3
m1350	67.9	24.6	2.5	0.2	1.9	1.3	1.0	0.3	0.3
m1450	69.0	25.2	2.6	0.2	0.7	1.2	0.5	0.3	0.3

	Ca	Si	Al	P	S	Mg	Na	Fe	Others
s 3:1	68.0	24.8	2.5	0.1	2.3	1.5	0.2	0.4	0.3
s p-200	68.2	24.5	2.5	0.0	2.4	1.4	0.3	0.3	0.3
s p-470	68.0	24.9	2.5	0.1	2.3	1.5	0.1	0.4	0.2
s m1350	67.8	25.0	2.6	0.2	1.9	1.4	0.6	0.3	0.3
s m1450	68.7	25.5	2.7	0.2	0.8	1.3	0.2	0.4	0.3

	Ca	Si	Al	P	S	Mg	Na	Fe	Others
h 3:1	68.0	24.5	2.6	0.2	1.9	1.9	0.4	0.4	0.3
h p-200	68.5	24.5	2.5	0.1	2.1	1.4	0.4	0.3	0.2
h p-470	68.5	24.3	2.5	0.1	2.0	1.8	0.2	0.4	0.3
h m1350	68.2	24.8	2.6	0.1	1.8	1.6	0.3	0.4	0.3
h m1450	68.9	25.4	2.7	0.2	0.7	1.1	0.3	0.3	0.3

Calcination:

- There is no significant changes in Ca, Si content
- Reduction in S

There is no significant changes in elemental composition after conventional or HIP sintering.

Figure 5D. Data for the Effect of sintering parameters on elemental composition of target

Figure 6A. Chart on the Effect of sintering parameters on phase composition of target

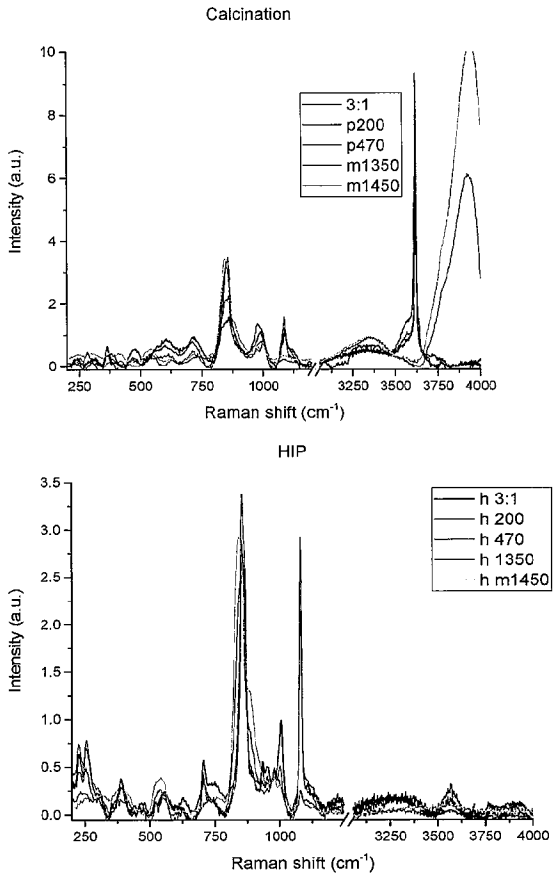

Figure 6B. Chart on the Effect of sintering parameters on phase composition of target

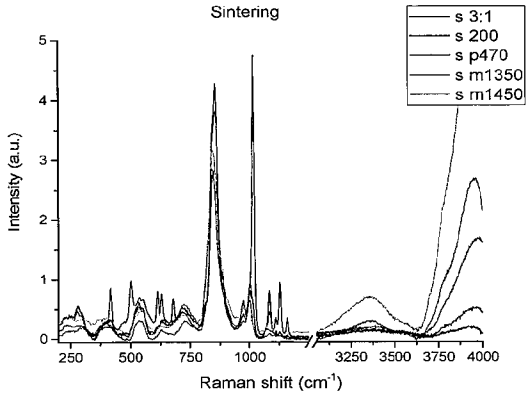

The melting process:

- removes hydrated phases, CaCO3 and CaSO4;
- partially transforms C3S to C2S

Figure 6C. Chart on the Effect of sintering parameters on phase composition of target

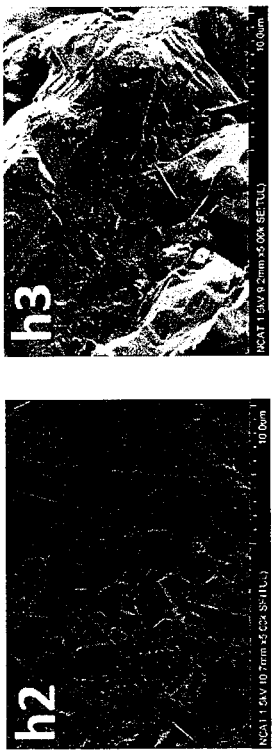

Figure 7A.

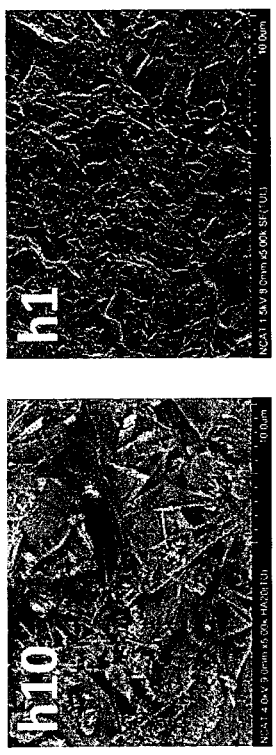

Figure 7B.

Figure 7C.

Figure 7D.

Figure 7E.

Figure 7F.

Figure 7G.

Figure 7I.

Figure 7H.

Sample #	Process Description
h10	Set tile, before sintering
h1	Hip sintered tile -700C, 15ksi,2hr
h2	Hip sintered tile -800C, 15ksi,2hr
h3	Hip sintered tile -900C, 20ksi,3hr
h4	Hip sintered tile -500C, 15ksi,2hr
h5	Hip sintered tile -700C, 15ksi,2hr
h7	Hip sintered tile -600C, 15ksi,2hr
1t	1p sintered (105C-30min; 450C-45min; 850C-4hr; 2.5 C/min)
2t	1p sintered (105C-1hr; 475C-1.5hr; 1000C-4hr; 2.5 C/min)

Figure 7J. Surface morphology of sintered targets.

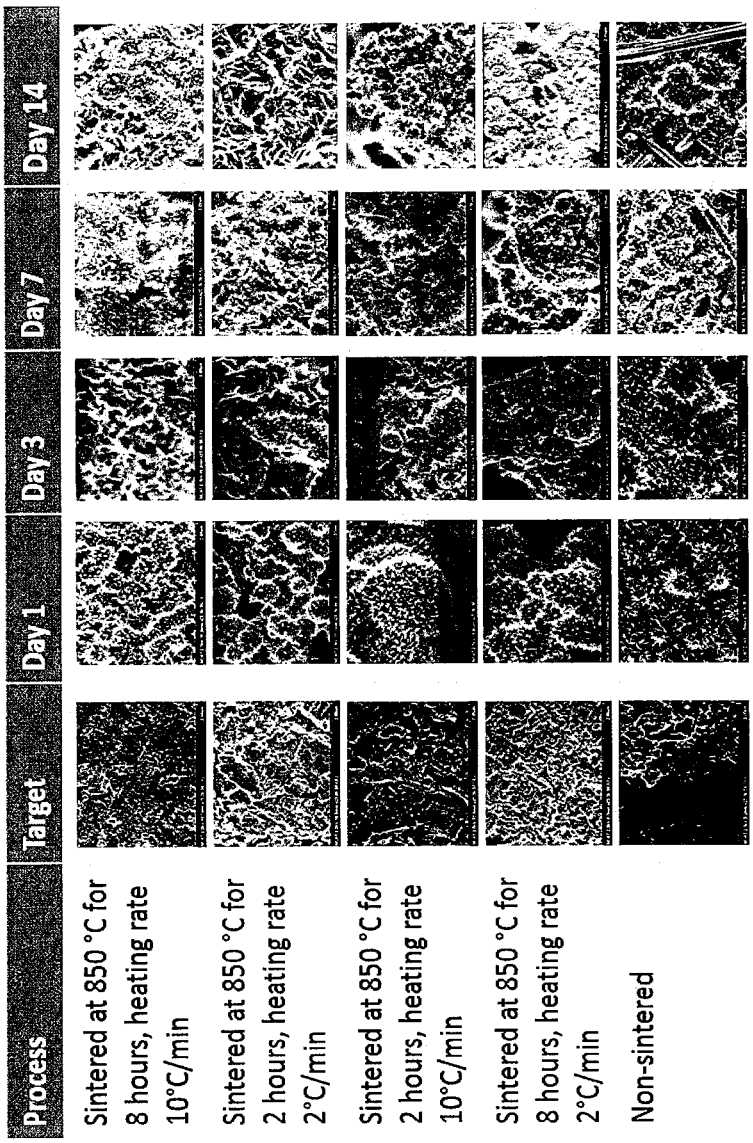

Figure 8A. Hydroxyapatite forming ability of sintered cement. The thermally treated cement produces 10 times more HA during immersion in PBS.

Figure 8B.

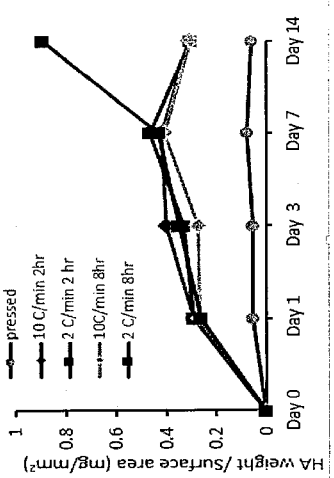

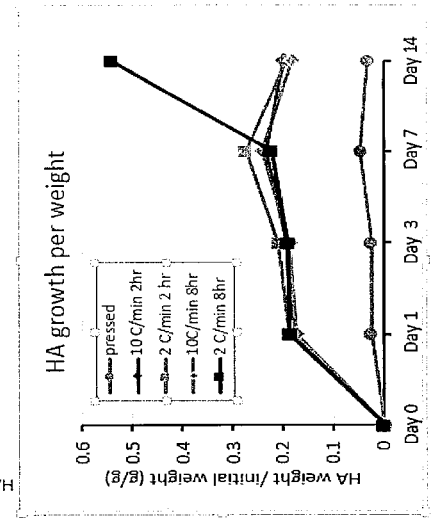

Figure 8C.

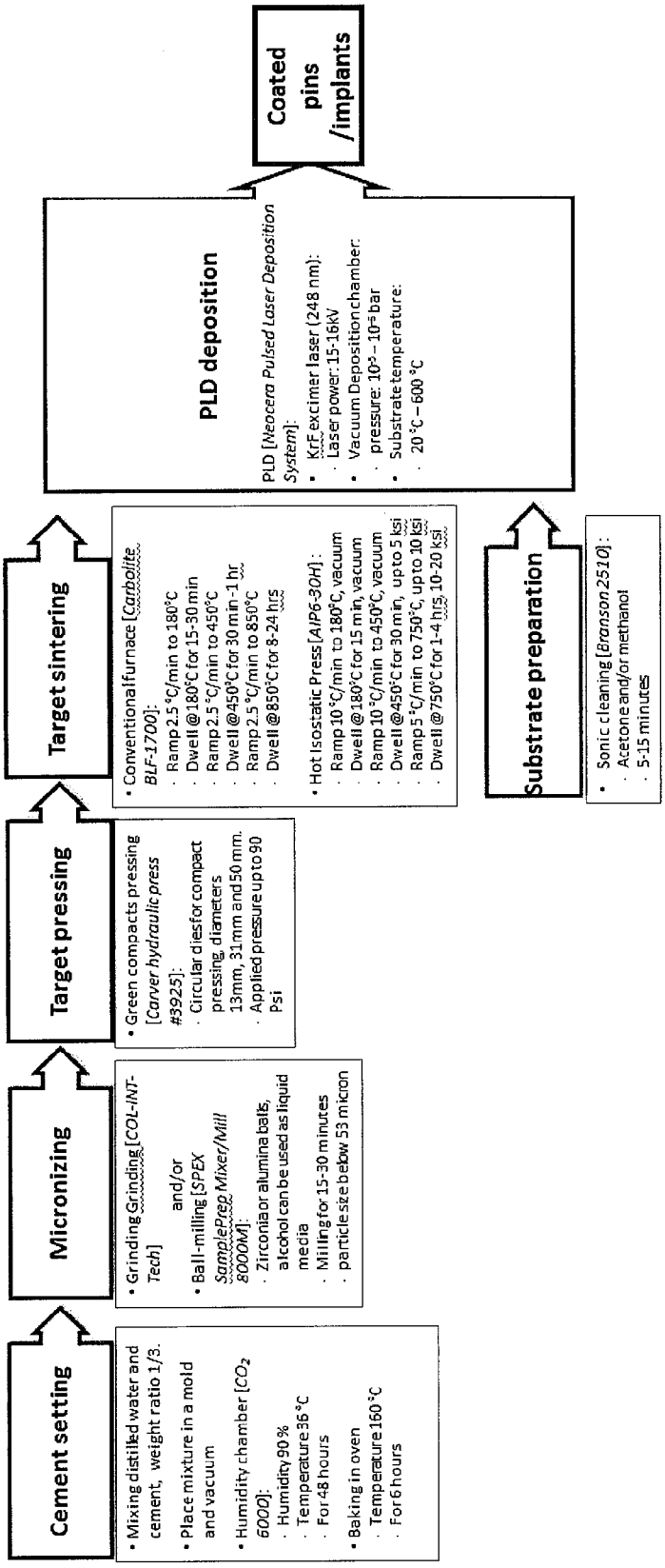

Figure 9 PLD process flow chart

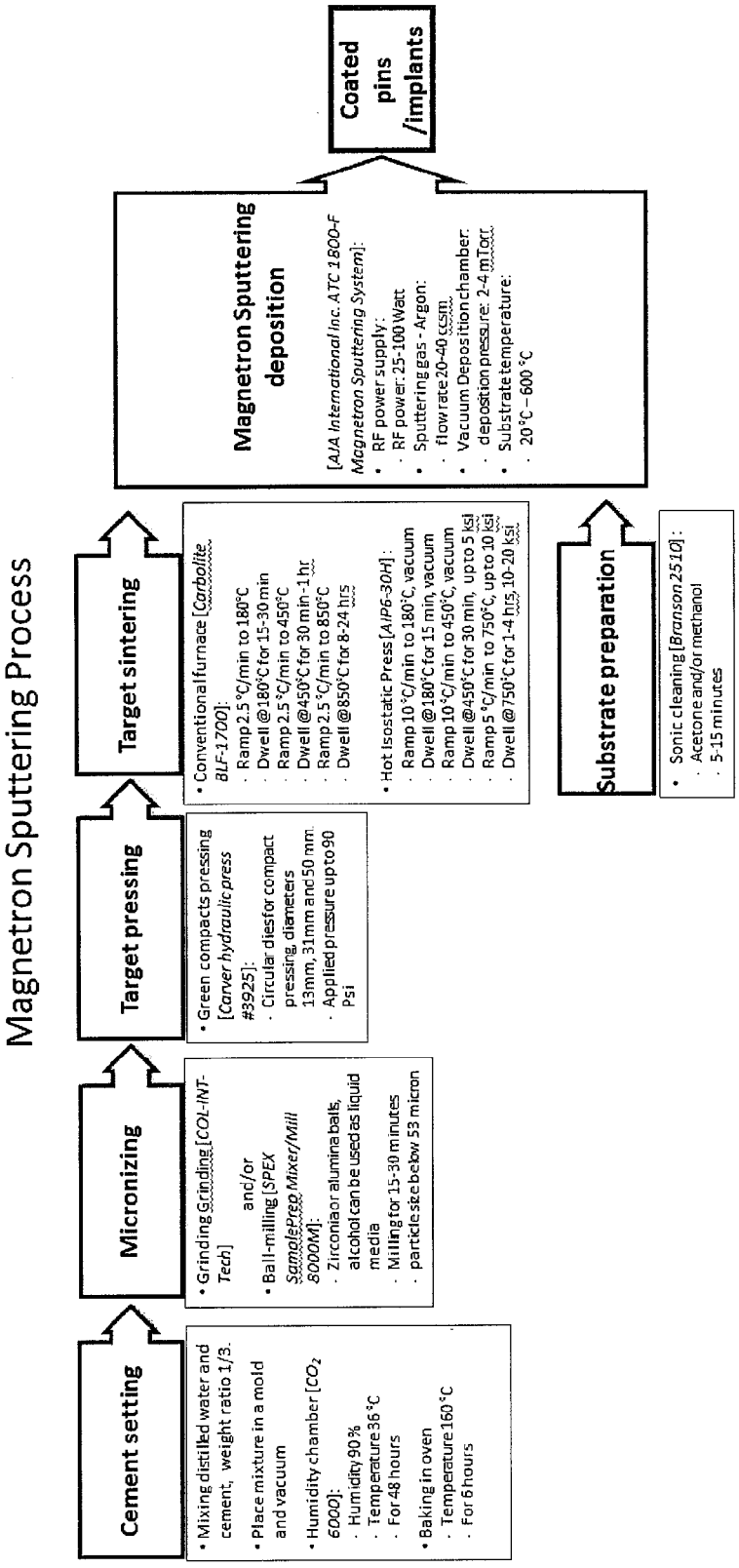

Figure 10. Magnetron Spattering process flow chart

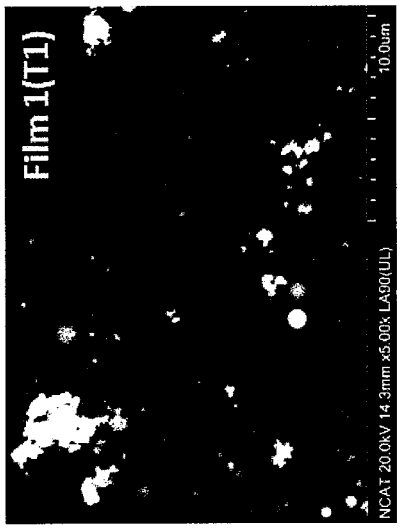

Figure 11A.

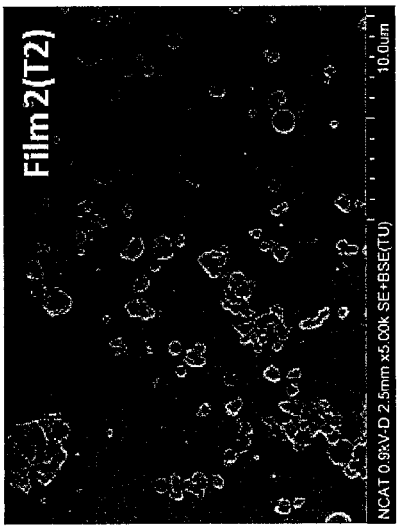

Figure 11B.

SEM Films on Si

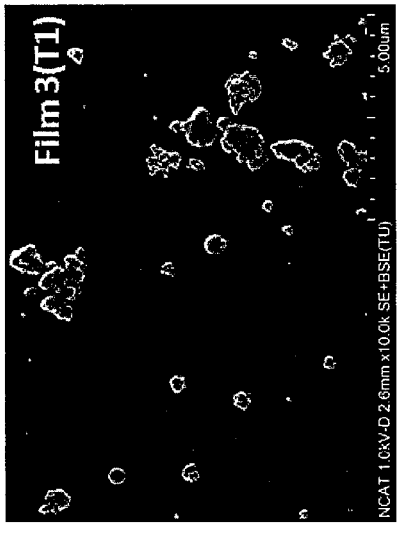

Figure 11C

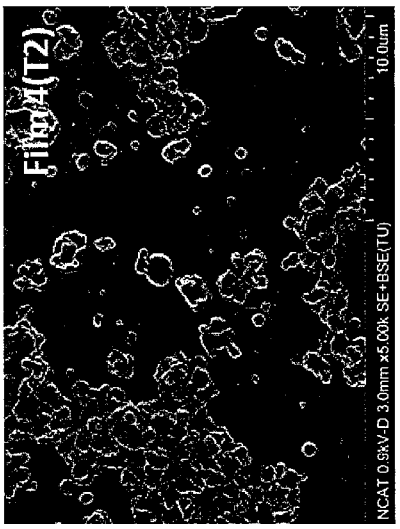

Figure 11D.

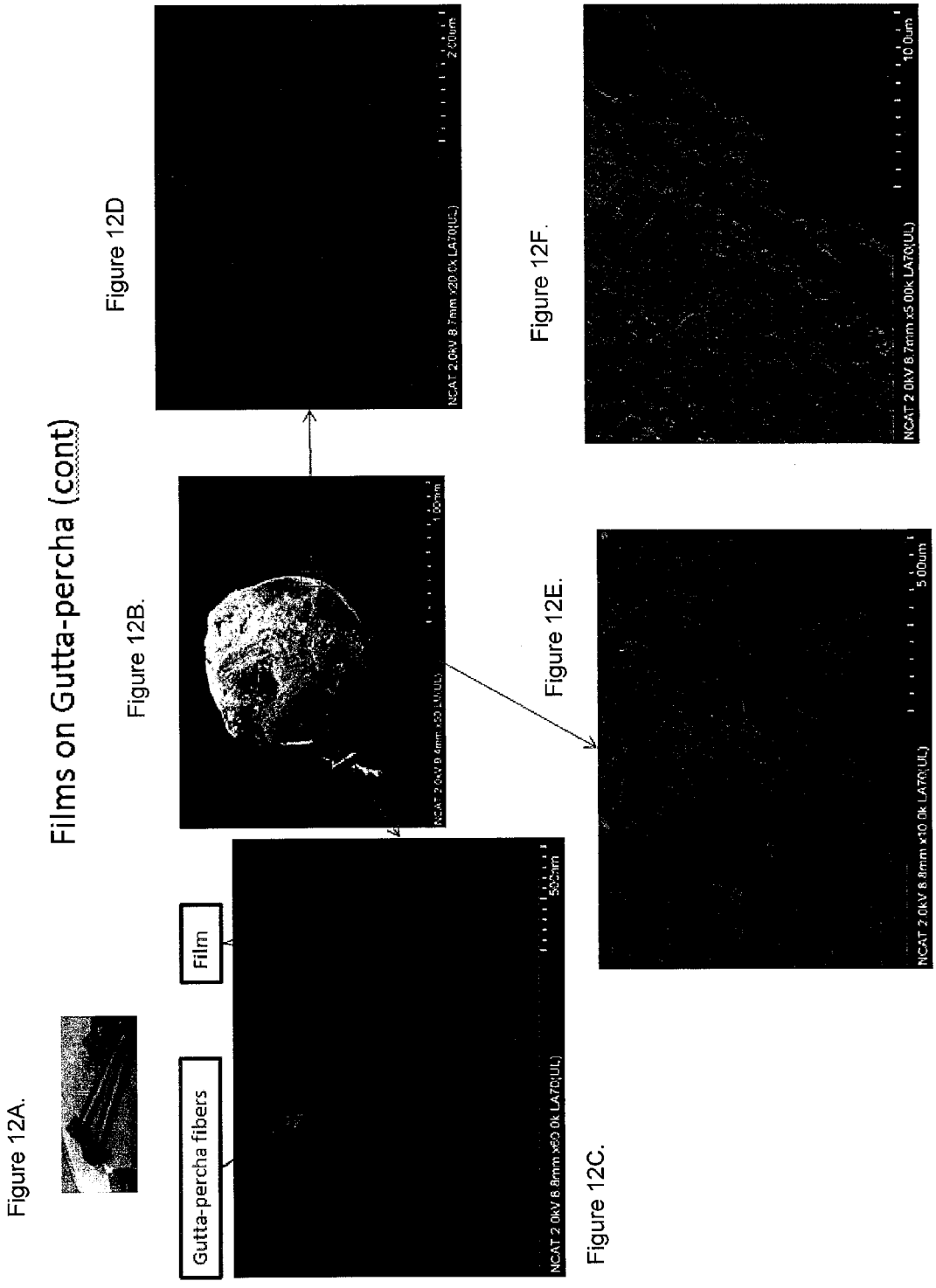
Films on Gutta-percha (cont)
Figure 12A.
Gutta-percha fibers
Film
Figure 12B.
Figure 12C.
Figure 12D
Figure 12E.
Figure 12F.

Figure 13A.

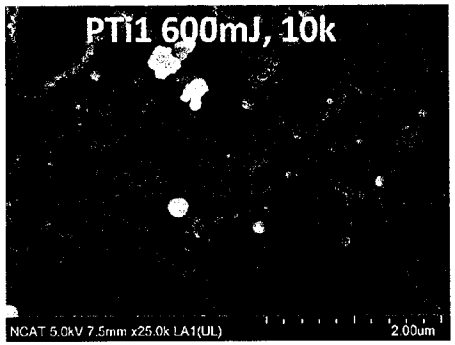

Figure 13B.

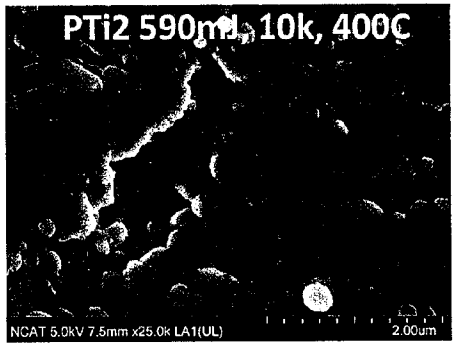

Figure 13C.

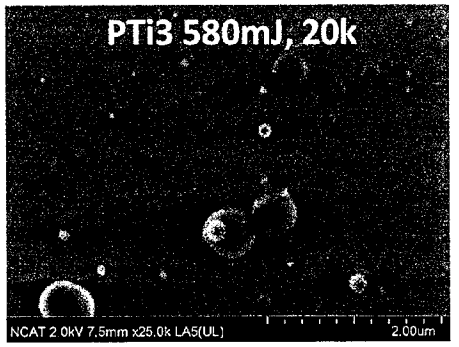

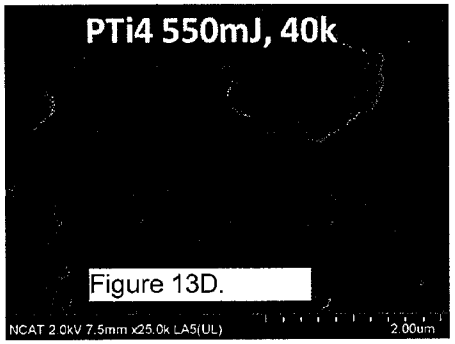

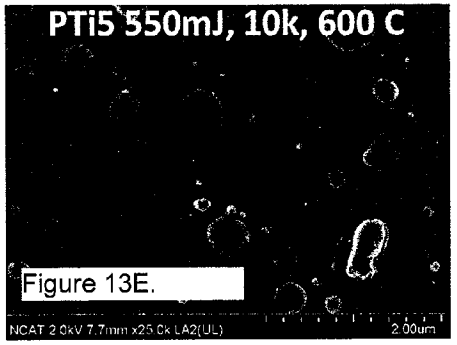

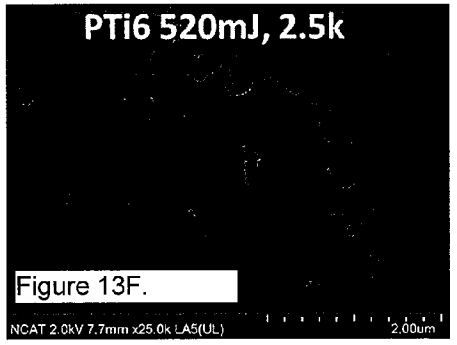

Sample #	Sample ID	Sample description	Q-ty	Process	Process parameters				Film Thickness (micron)			Average Roughness (microns)		
					Laser power	# Pulses	Substrate temperature	W pressure						
1	PTi1	PLD coating on Ti substrate	6	PLD	20kV, 600mJ	10000	RT	1.2 e-5 mbar	0.345	±	0.014	0.072	±	0.001
2	PTi2	PLD coating on Ti substrate	6	PLD	20kV, 590mJ	10000	400 C	7.5 e-5 mbar	0.398	±	0.034	0.091	±	0.009
3	PTi3	PLD coating on Ti substrate	6	PLD	20kV, 580mJ	20000	RT	1.2 e-5 mbar	0.577	±	0.034	0.103	±	0.009
4	PTi4	PLD coating on Ti substrate	6	PLD	20kV, 550mJ	40000	RT	1.2 e-5 mbar	1.025	±	0.054	0.124	±	0.015
5	PTi5	PLD coating on Ti substrate	6	PLD	21kV, 550mJ	10000	600 C	2.5 e-4 mbar	0.530	±	0.163	0.130	±	0.047
6	PTi6	PLD coating on Ti substrate	6	PLD	21kV, 520mJ	2500	RT	1.2 e-5 mbar	0.051	±	0.001	0.004	±	0.002

Figure 13G. Index of SEM images of films on titanium implants deposited by PLD process and table with process parameters.

Figure 14A.

Films characterization

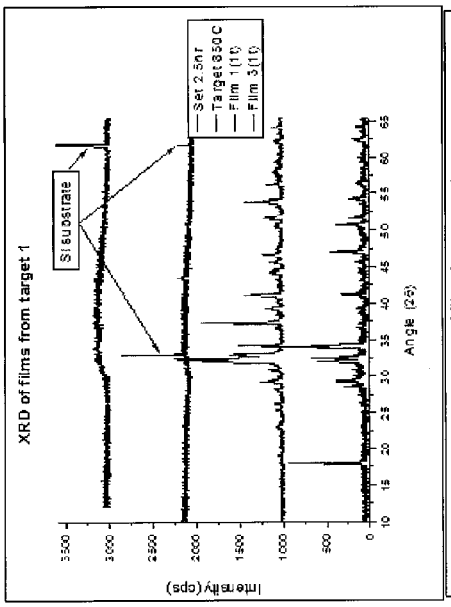

Figure 14B.

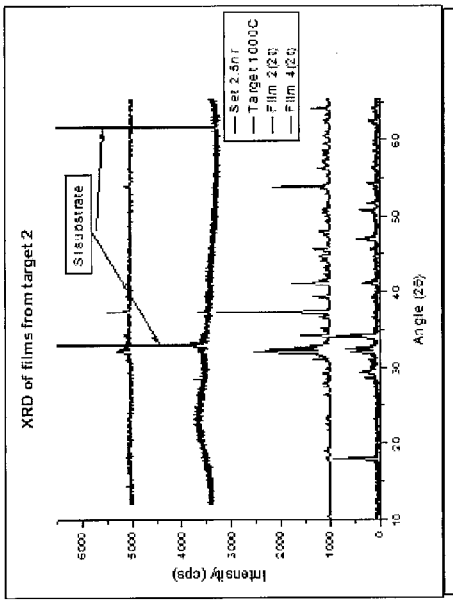

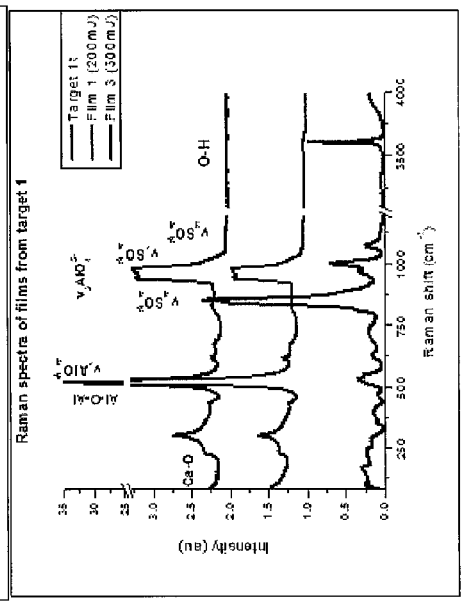

Figure 14C.

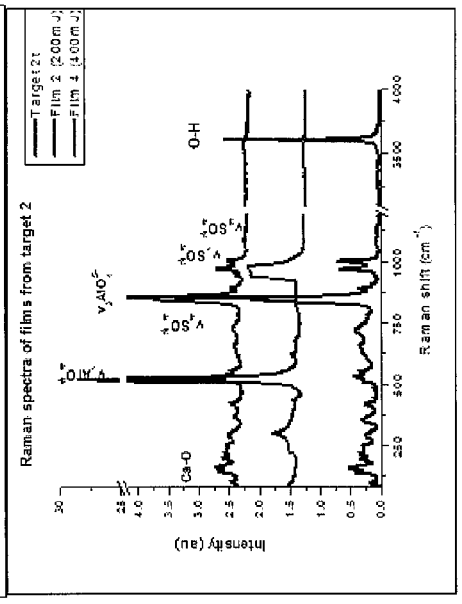

Figure 14D.

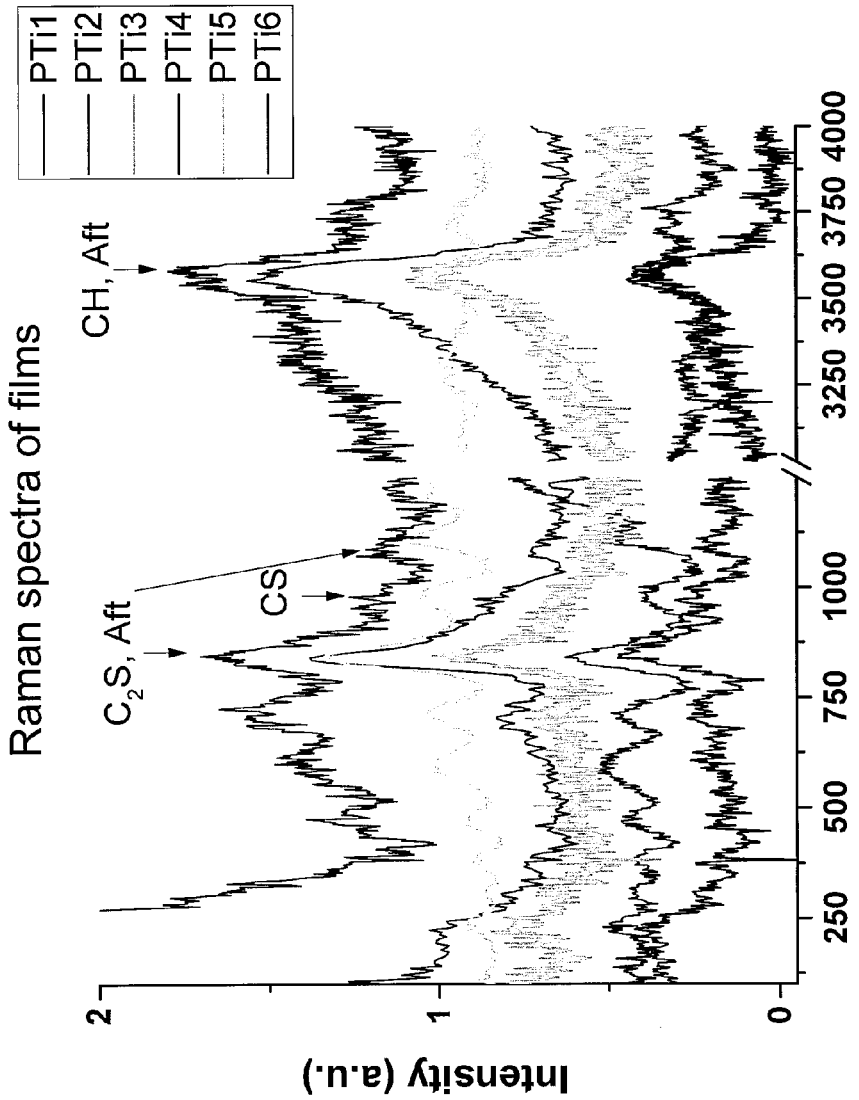

Figure 15. Raman analysis of films deposited on titanium implants using PLD process.

Elemental analysis of films: EDS , XRF

EDS elemental analysis of films

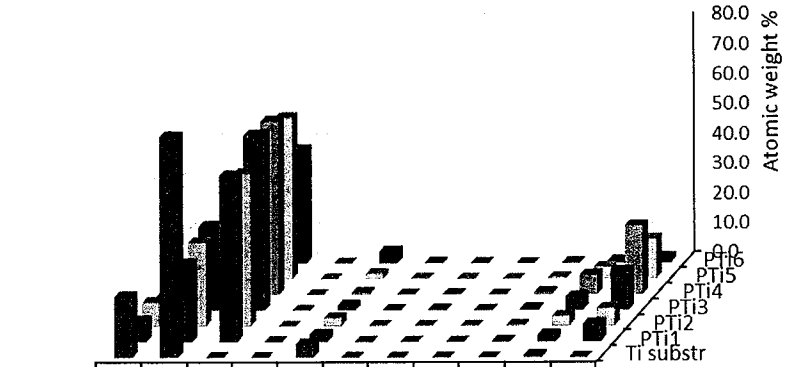

	Others	Ti	O	P	S	Fe	Mg	Na	Al	Si	Ca
Ti substr	20.4	74.1	0.0	0.0	4.6	0.0	0.0	0.0	0.0	0.9	0.1
PTi1	6.9	26.1	55.6	0.0	2.5	0.2	0.1	0.0	0.3	2.4	6.0
PTi2	8.0	28.0	51.1	0.0	2.7	0.2	0.2	0.1	0.4	3.3	6.0
PTi3	4.8	15.8	58.9	0.0	1.7	0.2	0.3	0.2	0.7	4.5	13.0
PTi4	4.5	5.6	58.3	0.0	0.7	0.1	0.3	0.0	0.9	6.5	23.0
PTi5	5.1	20.8	54.3	0.0	1.7	0.2	0.1	0.0	0.5	3.9	13.3
PTi6	12.3	42.9	38.1	0.0	3.9	0.2	0.0	0.0	0.1	0.7	1.8

Figure 16A. Elemental analysis of films deposited on titanium implants using PLD process.

XRF elemental analysis of films

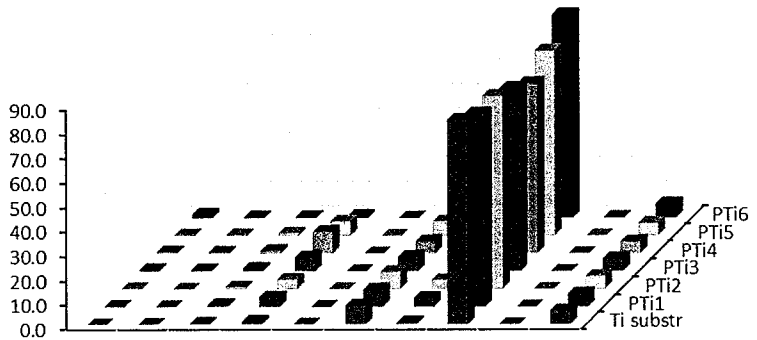

	Na	Mg	Al	Si	P	S	Ca	Ti	Fe	Others
Ti substr	0.0	0.1	0.6	1.4	0.1	7.8	0.9	83.6	0.0	5.7
PTi1	0.3	0.1	0.9	3.9	0.0	7.0	3.6	78.9	0.0	5.3
PTi2	0.3	0.1	0.9	3.9	0.0	7.0	3.6	78.9	0.0	5.3
PTi3	0.7	0.6	1.1	5.7	0.0	5.8	6.0	74.8	0.0	5.2
PTi4	0.6	0.6	1.2	8.8	0.0	4.9	9.4	69.6	0.0	4.8
PTi5	0.4	0.4	1.0	5.7	0.0	5.8	5.9	75.6	0.0	5.1
PTi6	1.5	0.2	0.4	0.9	0.0	7.1	1.4	82.8	0.1	5.7

Figure 16B. Elemental analysis of films deposited on titanium implants using PLD process.

HA formation

Set of films, deposited in the same conditions, and references (hydrated tile and targets) will be immersed in SBF (1x) at 37°C for 1, 3, 7, 14 and 21 days. After immersion the surface morphology of the samples and theirs composition will be investigated by SEM, XRD, and EDX/ XRF. We expect the formation of HA after 3–7 days of immersion, the crystallized fraction HA commonly reported after 14–21 days.

Figure 17A.

Figure 17B.

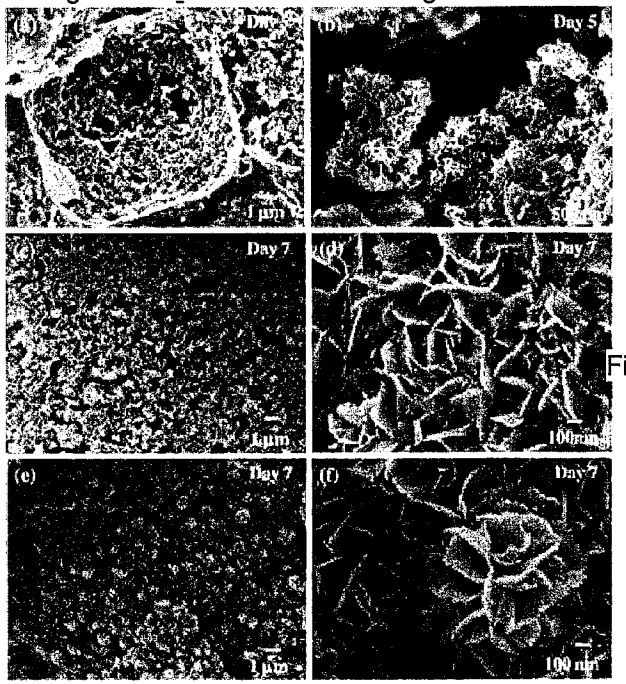

Figure 17C.

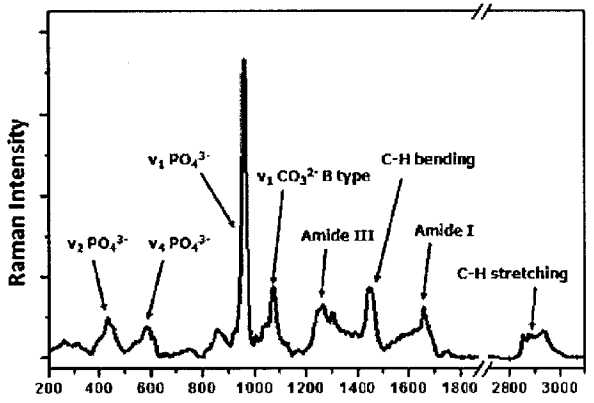

Figure 17D.

Buchwald, T., et al. (2012). "Identifying compositional and structural changes in spongy and subchondral bone from the hip joints of patients with osteoarthritis using Raman spectroscopy." Journal of Biomedical Optics 17(1): 0170071-0170077.

Nga, N. K., et al. "Biomimetic scaffolds based on hydroxyapatite nanorod/poly(D, L) lactic acid with their corresponding apatite-forming capability and biocompatibility for bone-tissue engineering." Colloids and Surfaces B: Biointerfaces(2015)

Figure 17E.

Figure 17F.

TABLE I
Calcium Phosphate Salts at Ambient Temperatures and Aquatic Solutions

Molecular Type	Ca/P Ratio	Name
$Ca(H_2PO_4)_2 \cdot H_2O$	0.50	Monohydrate calcium phosphate (MCPH)
$Ca(H_2PO_4)_2$	0.50	Monocalcium phosphate (MCP)
$CaHPO_4 \cdot 2\,H_2O$	1.00	Dicalcium phosphate dihydrate (DCPD)
α- and β- $Ca_3(PO_4)_2$	1.50	Tricalcium phosphate (TCP)
$Ca_4H(PO_4)_3 \cdot 2.5\,H_2O$	1.33	Octacalcium phosphate (OCP)
$Ca_5(PO_4)_3(OH)$	1.67	Hydroxyapatite (HAP)

Koutsopoulos, S. (2002). "Synthesis and characterization of hydroxyapatite crystals: A review study on the analytical methods." Journal of Biomedical Materials Research 62(4): 600-612.

Figure 17G Brief reference guide for HA-formation study.

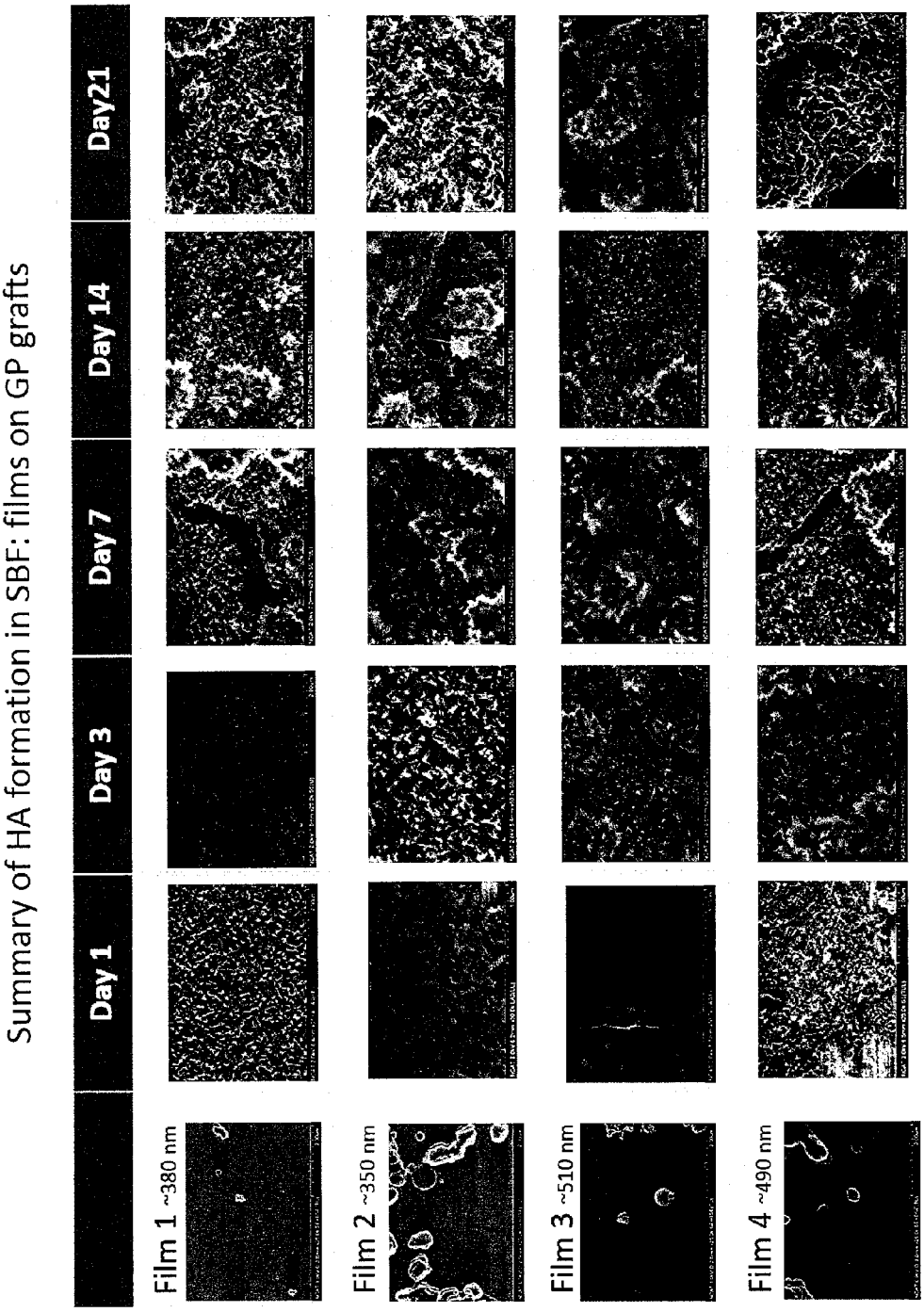

Figure 18. SEM observation of HA formation on films deposited on gutta-percha

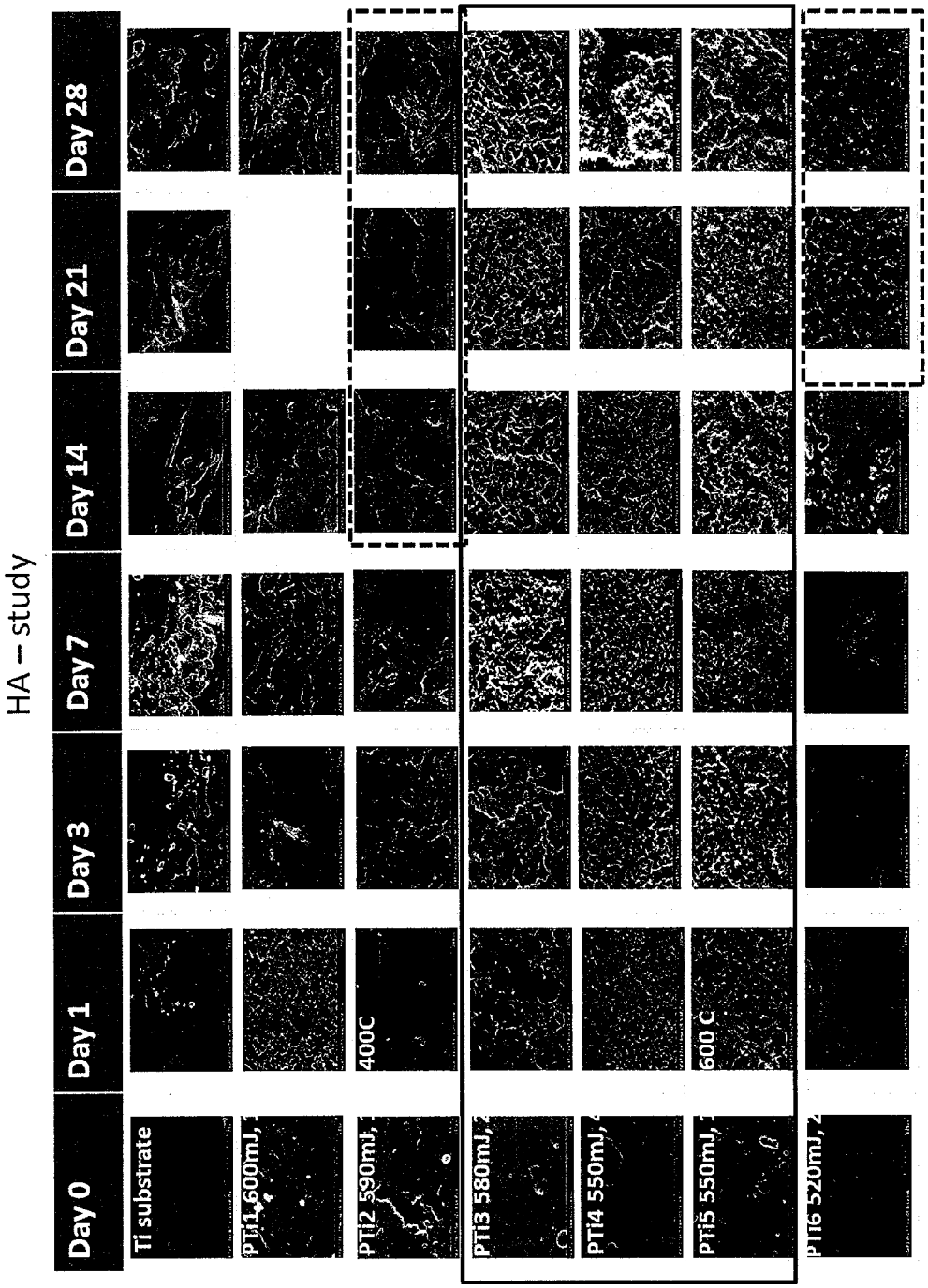

Figure 19 SEM observation of HA formation on films deposited on titanium (the best results highlighted in red)

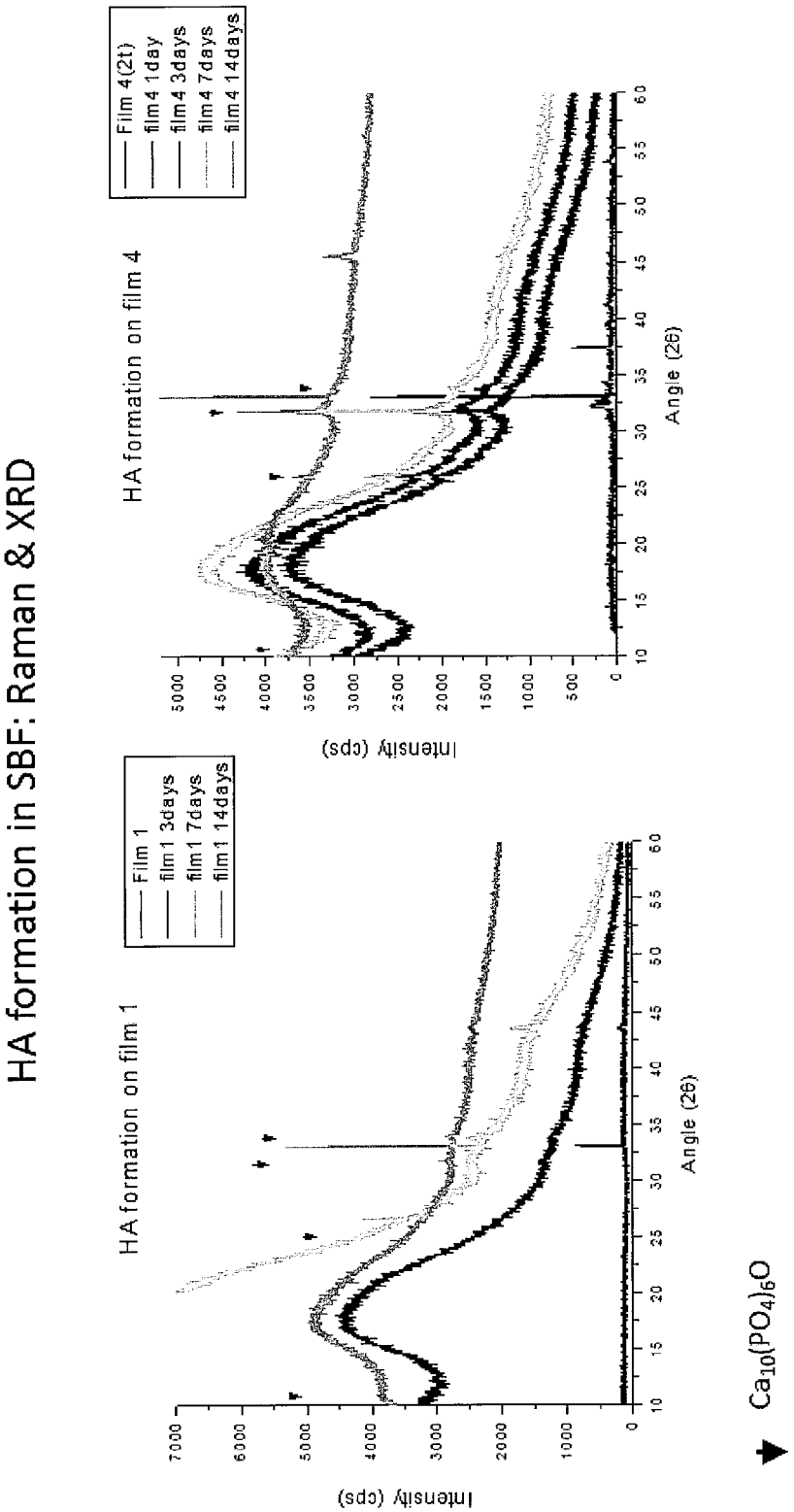

Figure 20A. Chart on the XRD analysis of HA formation on MTA coating deposited on gutta-percha.

Figure 20B. Chart on the XRD analysis of HA formation on MTA coating deposited on gutta-percha.

Figure 21A. Chart on the Raman analysis of HA formation on MTA coating deposited on titanium.

Figure 21B. Chart on the Raman analysis of HA formation on MTA coating deposited on titanium.

HA study:

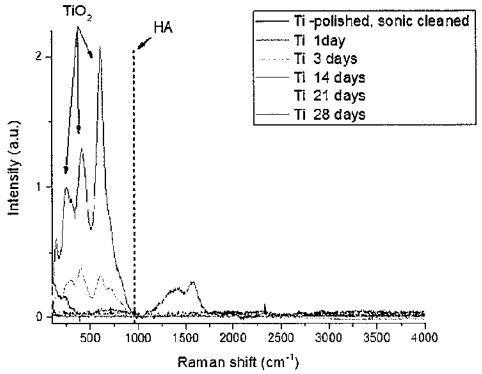

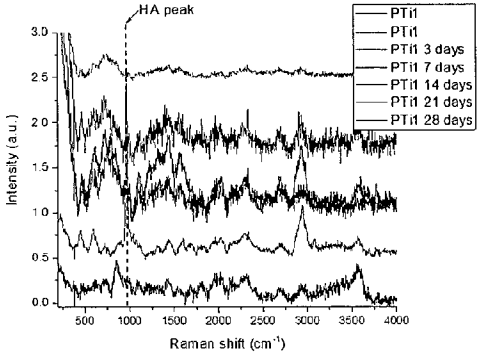

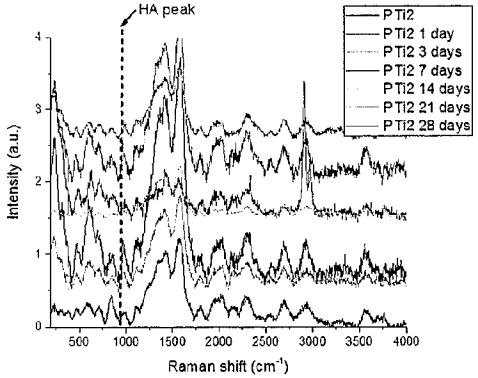

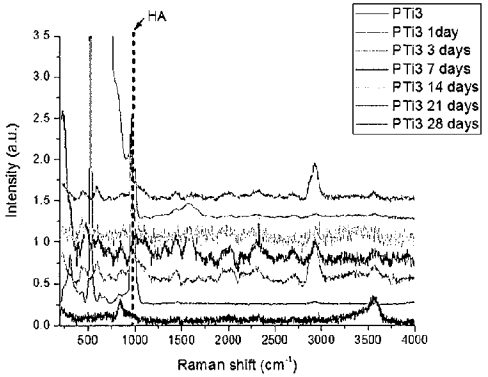

Figure 21C. Chart on the Raman analysis of HA formation on MTA coating deposited on titanium

Figure 21D. Chart on the Raman analysis of HA formation on MTA coating deposited on titanium.

Figure 21E. Chart on the Raman analysis of HA formation on MTA coating deposited on titanium.

Figure 21F. Chart on the Raman analysis of HA formation on MTA coating deposited on titanium.

HA study:

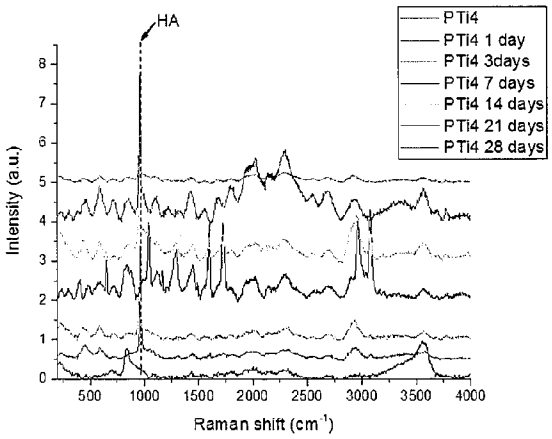

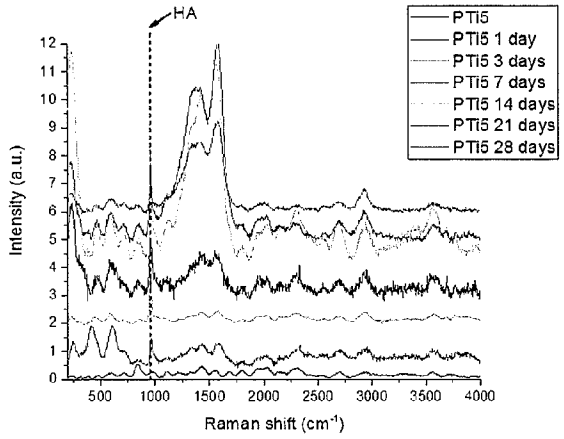

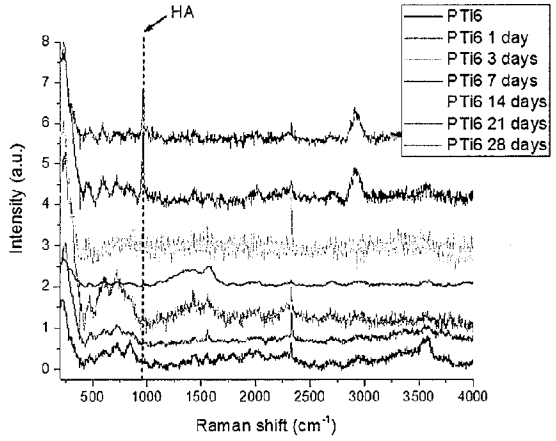

- Only films with thickness more than 500 nm shown stable HA growth from day 1.
- The HA were start forming on a thin film (PTi6, 50nm) after 3 weeks of immersion.

Figure 21G. Chart on the Raman analysis of HA formation on MTA coating deposited on titanium

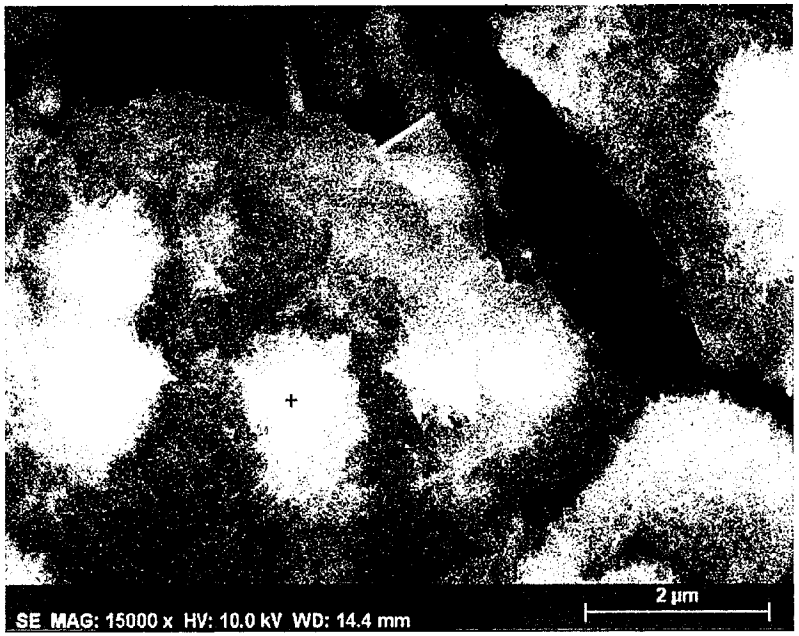

Figure 22A

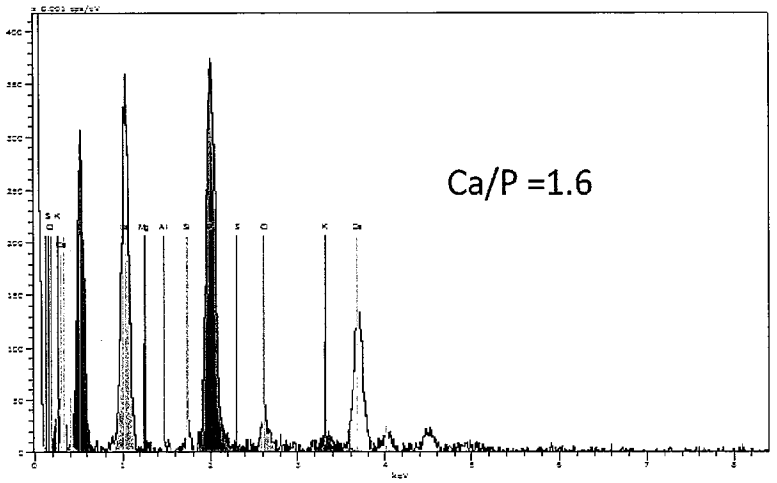

Spectrum: Acquisition

Element	Series	unn. C [wt.%]	norm. C [wt.%]	Atom. C [at.%]	Error [wt.%]
Oxygen	K-series	34.10	44.34	59.01	6.2
Sodium	K-series	16.45	21.39	9.81	1.2
Magnesium	K-series	0.14	0.18	0.16	0.1
Silicon	K-series	0.55	0.72	0.55	0.1
Phosphorus	K-series	12.58	16.36	11.25	0.6
Calcium	K-series	10.38	13.50	17.17	0.4
Chlorine	K-series	1.47	1.91	1.15	0.1
Aluminium	K-series	0.07	0.09	0.07	0.0
Sulfur	K-series	0.15	0.20	0.13	0.1
Potassium	K-series	1.01	1.31	0.72	0.1
	Total:	76.90	100.00	100.00	

Figure 22B. Chart on the EDS spectra of HA formed on MTA coating deposited on gutta-percha

Figure 23A.

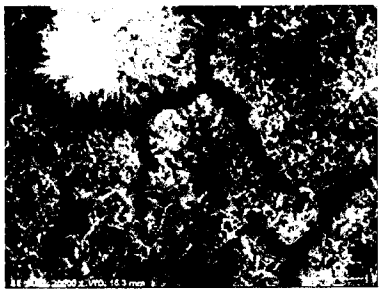

HA formation:
The elemental maps clearly shown that Ca, P and O create a similar patterns. At the same time the Na doesn't have distribution similar to P therefore we can conclude that major component is calcium phosphates.

Figure 23C.

Figure 23B.

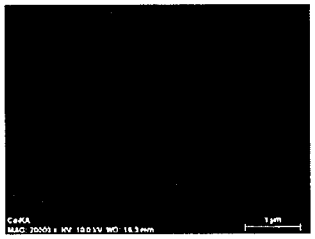

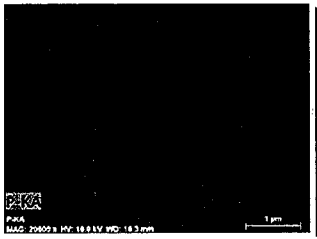

Figure 23D.

Figure 23E.

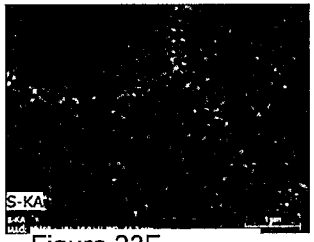

Figure 23G.

Figure 23F.

Figure 23H.

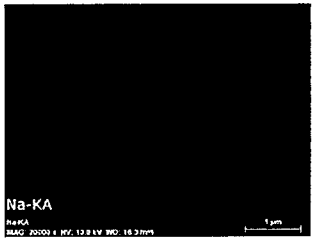

Figure 23I.

Appendix I: HA study - day 1

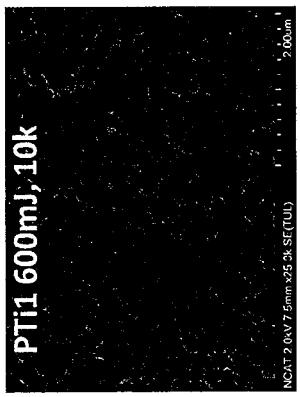

Figure 24A.

Figure 24B.

Figure 24C.

Figure 24D.

Figure 24E.

Figure 24F.

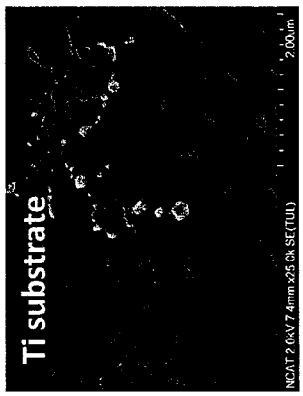

Figure 24G.

Appendix I: HA study - day 3

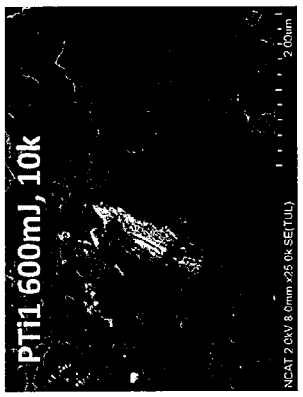

Figure 25A.

Figure 25B.

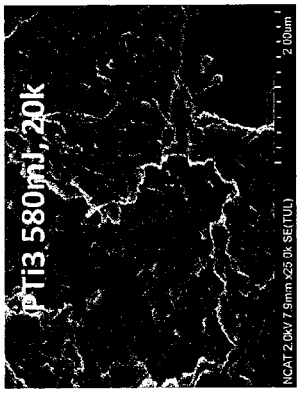

Figure 25C.

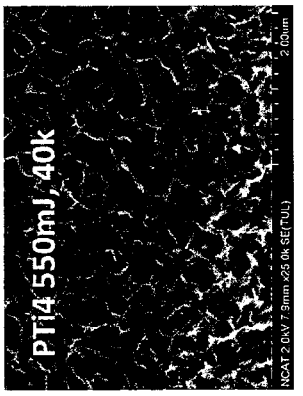

Figure 25D.

Figure 25E.

Figure 25F.

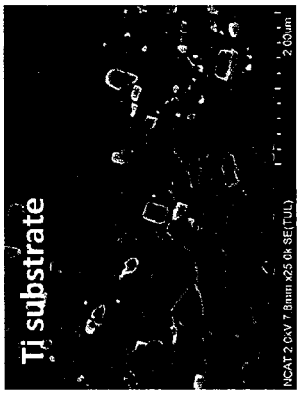

Figure 25G.

Appendix I: HA study - day 7

Figure 26A.

Figure 26B.

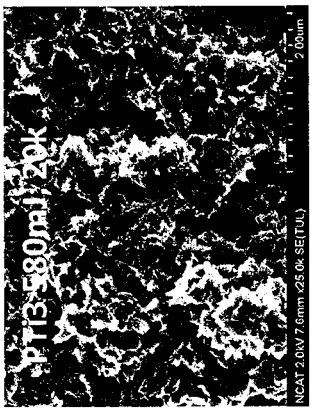

Figure 26C.

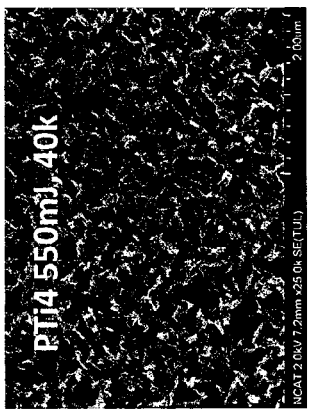

Figure 26D.

Figure 26E.

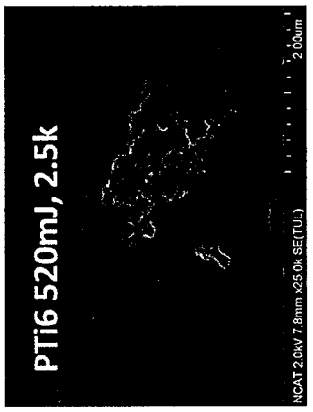

Figure 26F.

Figure 26G.

Appendix I: HA study - day 14

Figure 27A.

Figure 27B.

Figure 27C.

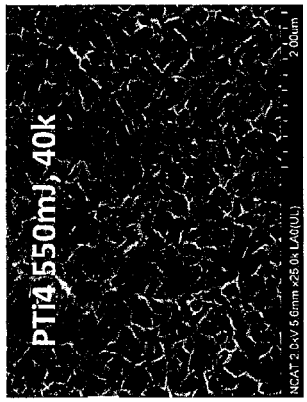

Figure 27D.

Figure 27E.

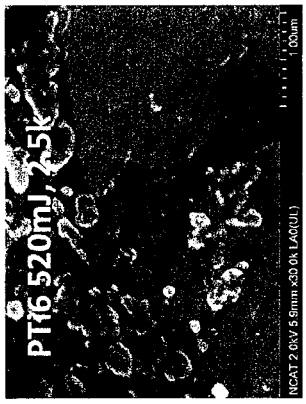

Figure 27F.

Figure 27G.

Appendix I: HA study - day 21

Figure 28A.

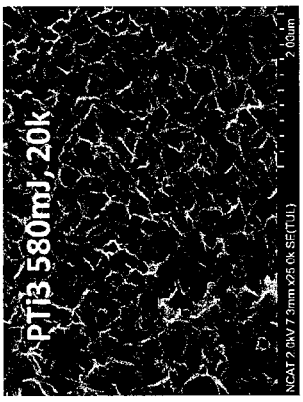

Figure 28B.

Figure 28D.

Figure 28E.

Figure 28C.

Figure 28F.

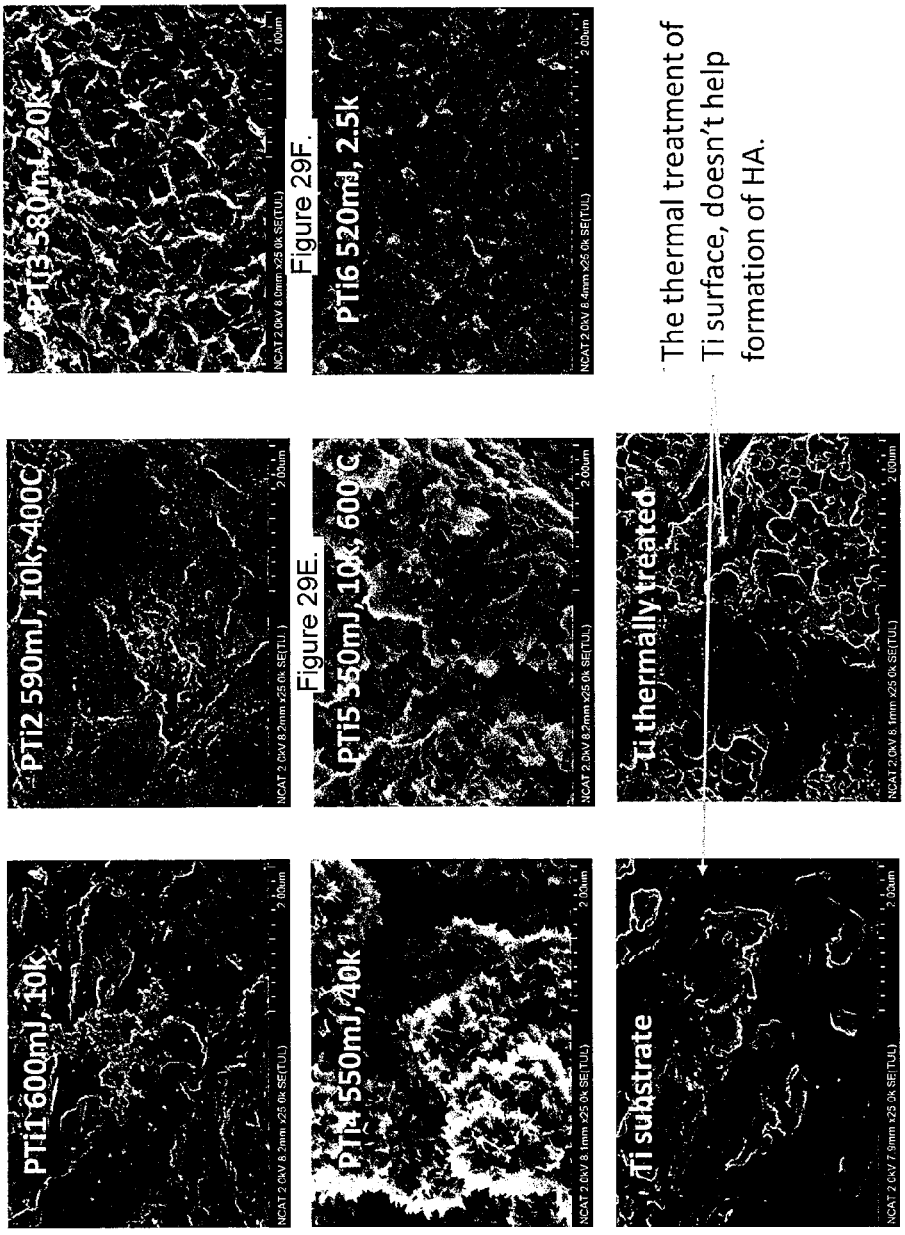

Figure 29A.

Figure 29B.

Figure 29C.

Figure 29D.

Figure 29E.

Figure 29F.

Figure 29G.

Figure 29H.

Appendix II: EDS Results of HA formation study

Figure 30A.

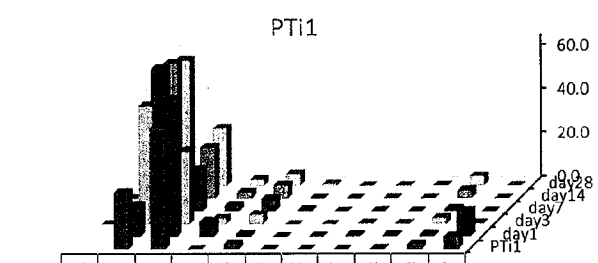

	Cl	Ti	O	P	S	Fe	Mg	Na	Al	Si	Ca
PTi1		26.1	55.6	0.0	2.5	0.2	0.1	0.0	0.3	2.4	6.0
day1		14.3	62.7	7.1	1.3	0.0	0.1	0.8	0.7	1.2	11.7
day3	0.1	54.2	33.3	2.7	4.5	0.0	0.0	0.5	0.3	2.9	0.5
day7	0.1	69.0	18.8	2.7	5.7	0.8	0.0	0.2	0.0	1.2	0.0
day14	0.2	61.7	23.4	3.1	6.2	0.1	0.1	0.2	0.2	3.8	0.0
day28	0.3	57.5	26.5	3.1	5.6	0.9	0.0	0.2	0.3	4.5	0.0

Figure 30B.

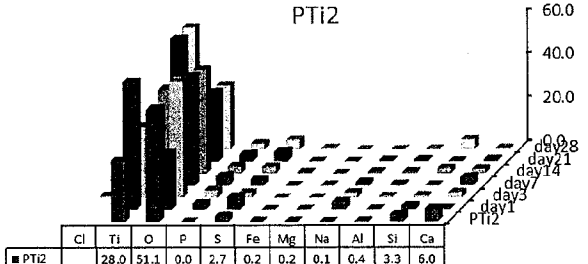

	Cl	Ti	O	P	S	Fe	Mg	Na	Al	Si	Ca
PTi2		28.0	51.1	0.0	2.7	0.2	0.2	0.1	0.4	3.3	6.0
day1		58.4	25.9	3.0	5.8	0.0	0.2	3.7	0.3	1.9	0.8
day3	0.9	32.7	53.3	3.5	2.4	0.0	0.0	2.4	0.7	1.0	2.3
day7		35.3	49.8	4.3	2.9	0.1	0.1	1.6	0.7	0.2	3.8
day14	0.0	38.7	47.3	3.4	3.1	0.6	0.0	0.7	0.9	2.5	2.2
day21	0.2	56.0	31.4	3.3	4.7	0.3	0.0	0.8	0.9	0.2	1.0
day28	0.1	55.9	29.3	2.8	4.6	0.7	0.0	0.2	0.3	4.7	0.6

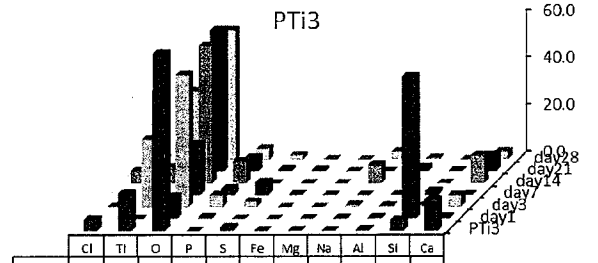

	Cl	Ti	O	P	S	Fe	Mg	Na	Al	Si	Ca
PTi3	4.8	15.8	58.9	0.0	1.7	0.2	0.3	0.2	0.7	4.5	13.0
day1		0.0	9.2	0.7	0.0	0.0	0.1	0.4	0.6	88.1	0.8
day3	0.3	28.6	55.9	5.1	2.3	0.0	0.1	1.0	0.6	0.7	5.1
day7	0.0	66.5	21.4	2.9	5.5	0.5	0.0	0.1	0.2	1.7	0.1
day14	5.3	6.7	58.1	9.4	0.0	0.0	0.0	8.0	0.6	0.0	11.9
day21	0.3	5.7	75.8	5.7	1.0	0.8	0.0	0.1	1.7	0.3	7.0
day28	0.8	29.0	55.0	4.8	2.0	0.3	0.0	3.5	0.7	0.1	3.5

Figure 30C.

The EDS analysis shows the tendency in dissolution of films. It could be detected by increased amount of Ti and reduction of Si content.

The precipitation of several salts, including hydroxyapatite could be observed by variation in amount of Ca, P, Na and Cl content.

It could be seen that films with the best performance (PTi3, PTi4 and PTi5) have higher content of Ca.

Appendix II: EDS Results of HA formation study (continued)

Figure 30D.

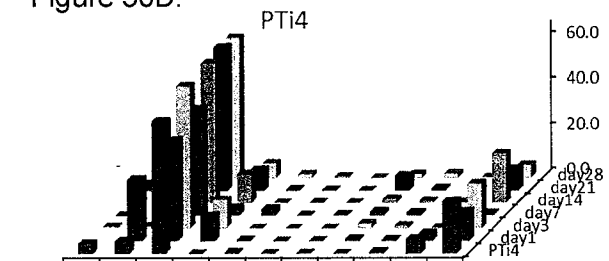

	Cl	Ti	O	P	S	Fe	Mg	Na	Al	Si	Ca
PTi4	4.5	5.6	58.3	0.0	0.7	0.1	0.3	0.0	0.9	6.5	23.0
day1		27.2	44.0	10.9	0.4	0.0	0.2	1.0	0.6	3.2	12.7
day3	0.7	0.9	62.5	12.6	0.0	0.0	0.1	2.1	1.1	0.2	19.7
day7	0.1	41.0	46.8	3.3	2.9	0.1	0.4	1.7	1.3	0.5	1.0
day14	0.3	0.7	61.3	12.7	0.0	0.2	0.1	1.8	0.9	0.2	21.7
day21	2.8	8.1	62.5	8.8	0.6	0.2	0.0	6.5	1.0	0.1	9.2
day28	0.3	20.3	61.3	6.4	1.6	0.5	0.0	1.6	1.9	0.1	5.5

Figure 30E.

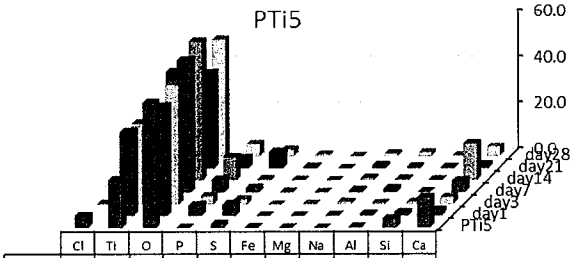

	Cl	Ti	O	P	S	Fe	Mg	Na	Al	Si	Ca
PTi5	5.1	20.8	54.3	0.0	1.7	0.2	0.1	0.0	0.5	3.9	13.3
day1		36.7	47.5	4.7	5.3	0.0	0.1	0.2	1.1	1.7	2.7
day3	0.4	35.1	51.4	3.5	2.2	0.0	0.2	1.0	0.5	1.0	3.1
day7	0.1	26.9	57.0	5.4	2.0	0.2	0.1	1.0	1.7	0.2	4.9
day14	0.5	9.5	61.1	10.0	0.6	0.1	0.0	1.0	0.6	0.3	16.1
day21	0.3	41.7	41.1	4.3	7.1	0.7	0.0	1.3	0.6	0.4	1.5
day28	0.1	32.3	50.5	5.6	2.9	0.7	0.1	1.2	1.7	0.3	4.2

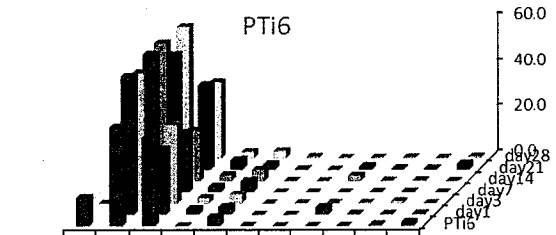

	Cl	Ti	O	P	S	Fe	Mg	Na	Al	Si	Ca
PTi6	12.3	42.9	38.1	0.0	3.9	0.2	0.0	0.0	0.1	0.7	1.8
day1		61.4	28.2	2.6	3.5	0.0	0.0	3.3	0.4	0.2	0.5
day3	0.1	56.7	34.3	2.4	4.0	0.0	0.1	0.2	0.2	0.9	0.0
day7	0.0	65.4	25.4	2.6	5.0	0.0	0.0	0.0	0.2	0.4	0.0
day14	1.3	64.9	21.8	2.6	4.9	0.1	0.1	2.4	0.2	0.4	0.0
day21	0.3	49.8	36.8	4.1	2.4	0.3	0.0	1.5	0.5	0.4	2.6
day28	0.0	57.2	33.2	2.9	3.2	0.7	0.1	0.3	0.3	0.2	0.7

Figure 30F

Appendix II: EDS maps (film before immersion, PTi-5)

Figure 31A.

Figure 32A.

Figure 31J.

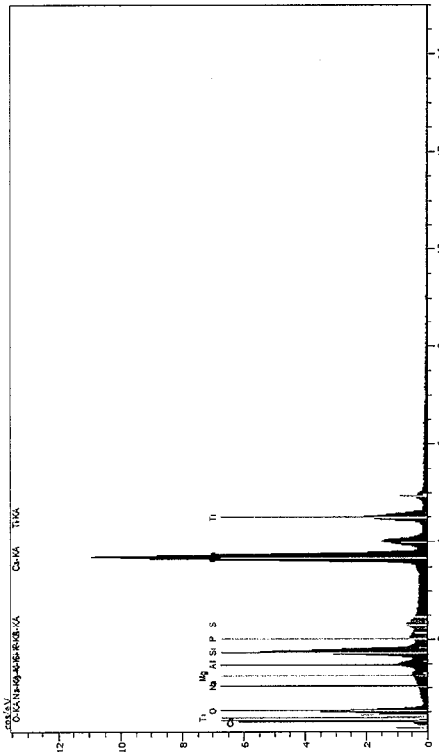

Figure 31B.

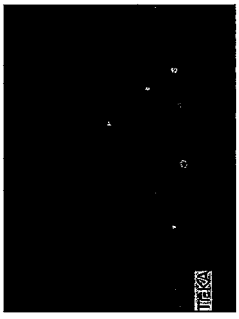

Figure 31C.

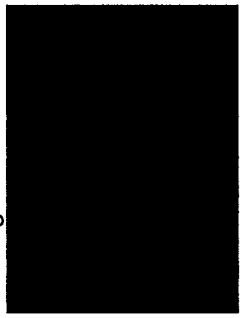

Figure 31D.

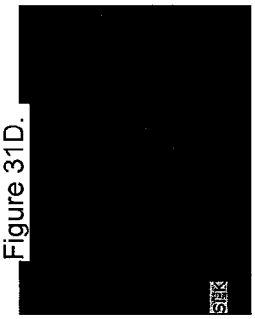

Figure 31E.

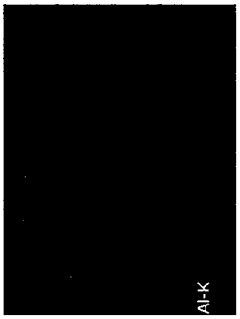

Figure 31F

Figure 31G.

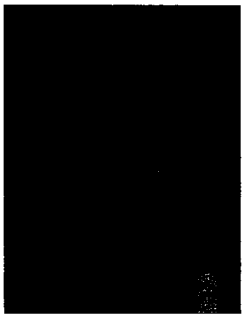

Figure 31H.

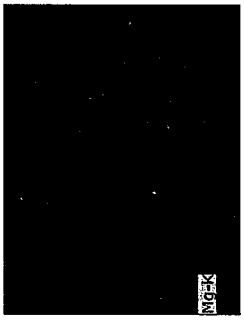

Figure 32I.

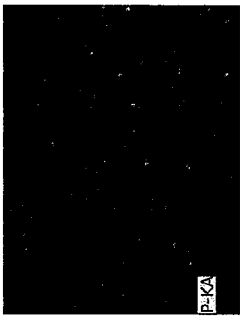

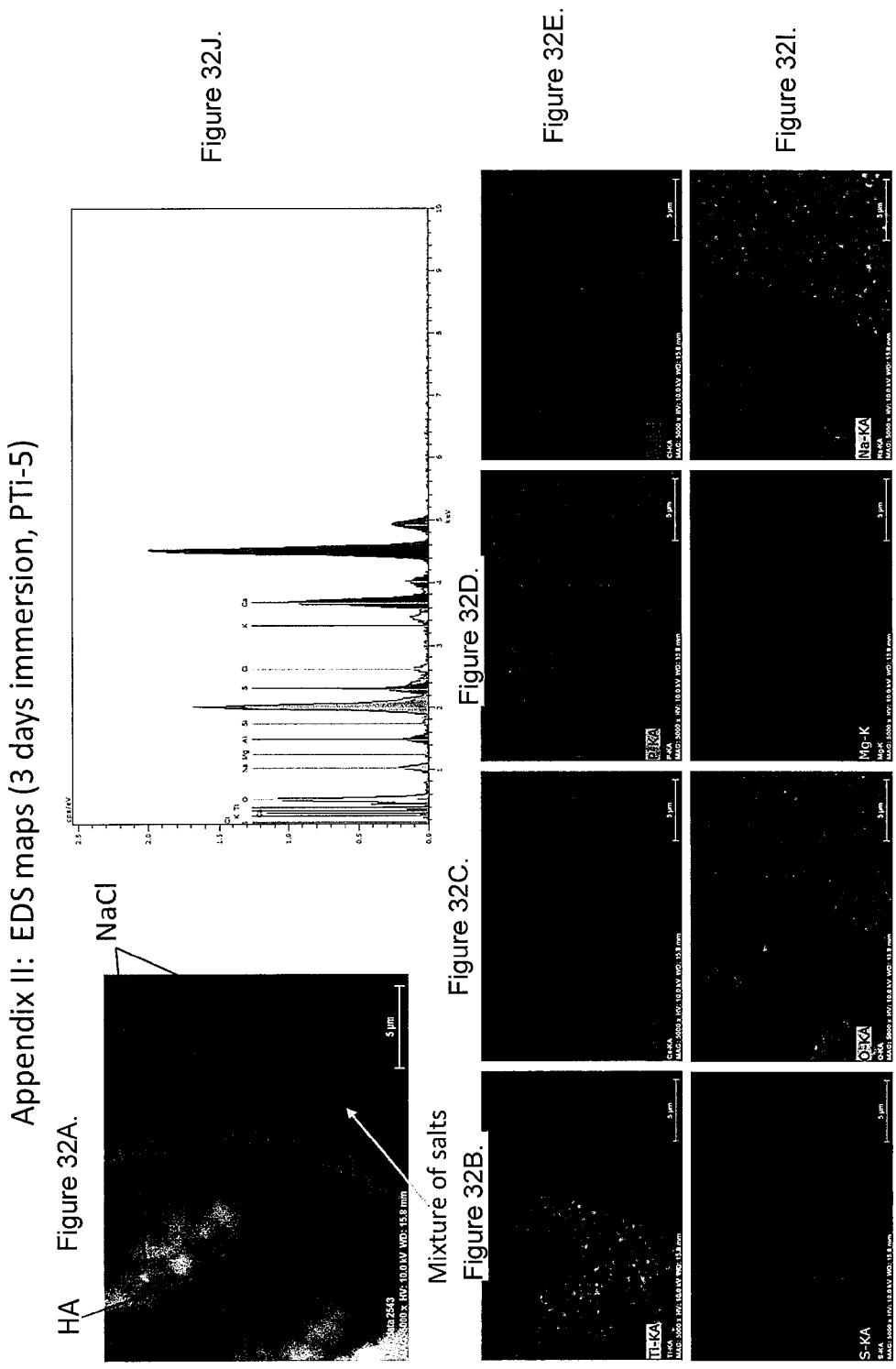
Appendix II: EDS maps (3 days immersion, PTi-5)
HA
Figure 32A.
NaCl
Figure 32J.
Mixture of salts
Figure 32B.
Figure 32C.
Figure 32D.
Figure 32E.
Figure 32F
Figure 32G.
Figure 32H.
Figure 32I.

METHOD FOR CREATING A MINERAL TRIOXIDE AGGREGATE MATERIAL WITH IMPROVED BIOLOGICAL EFFECTS

RELATED U.S. APPLICATION DATA

[0001] This application is a non-provisional claiming priority to pending provisional U.S. Pat. App. Ser. No. 62/154,282 filed on Apr. 29, 2015.

FIELD OF INVENTION

[0002] The present invention relates to the process of creating an improved biological Mineral Trioxide Aggregate (MTA) in a dense tile, or Target. The Target enables a process of coating the improved MTA on implantable medical devices or can be micronized into a MTA material for traditional use.

BACKGROUND OF THE INVENTION

[0003] Mineral trioxide aggregate (MTA) (sold under the trade names gray or white ProRoot MTA (Dentsply Sirona Inc., York, Pa., US) is a substance currently used in general dentistry and in endodontics to replace natural tooth material in apexification, pulp capping, pulpotomy, regenerative endodontics, root canal filling, root-end filling, root perforation repair, tooth restorations and the like. An example of MTA used in endodontic applications is disclosed in U.S. Pat. No. 8,979,991 which is hereby incorporated by reference for such disclosure.

[0004] It would be desirable to provide an MTA material for dental applications including for endodontic, restorative or other uses, that has improved biological effect. More particularly, it would be beneficial to the dental arts to provide such a material that is demonstrated to improve the production of hydroxyl apatite (HA) in the presence of body fluids (or simulated body fluids such as phosphate buffered saline) to produce a material having cementum qualities.

[0005] For example, in endodontic applications, the material or composition should provide a stable barrier to bacteria and fluid leakage in the root canal system of a tooth. In addition, the composition should help promote the growth of the new bone and tissue surrounding the root tip area.

BRIEF DESCRIPTION OF THE DRAWINGS

[0006] FIG. **1** includes a flowchart of a target preparation process;

[0007] FIG. **2**A includes a table providing data of the effects of sintering parameters on target density;

[0008] FIG. **2**B includes a chart representing the effect of sintering parameters on targets density shown in the table of FIG. **2**A;

[0009] FIG. **3**A includes a chart representing the effect of HIP process parameters on targets density;

[0010] FIG. **3**B includes a chart representing the effect of pre-calcination on targets density;

[0011] FIG. **4**A includes a chart representing the effect of sintering parameters on mechanical properties on target;

[0012] FIG. **4**B includes a chart representing the effects of sintering parameters on mechanical properties on target;

[0013] FIG. **4**C includes a photo of various samples on a target to show the effect of sintering parameters on mechanical properties on the target;

[0014] FIG. **5**A includes a chart representing the effects of elemental composition of pre-sintered target;

[0015] FIG. **5**B includes a chart on the effects of elemental composition of a conventional sintered target;

[0016] FIG. **5**C includes a chart on the effects of elemental composition of a HIP sintered target;

[0017] FIG. **5**D includes a table representing the data of the effects of sintering parameters on elemental composition of target;

[0018] FIG. **6**A includes a chart representing the effect of sintering parameters on phase composition of target;

[0019] FIG. **6**B includes a chart representing the effect of sintering parameters on phase composition of target;

[0020] FIG. **6**C includes charts representing the effect of sintering parameters on phase composition of target;

[0021] FIG. **7**A includes a photo representing surface morphology of a sintered target;

[0022] FIG. **7**B includes a photo representing surface morphology of another sintered target;

[0023] FIG. **7**C includes a photo representing surface morphology of another sintered target;

[0024] FIG. **7**D includes a photo representing surface morphology of another sintered target;

[0025] FIG. **7**E includes a photo representing surface morphology of another sintered target;

[0026] FIG. **7**F includes a photo representing surface morphology of another sintered target;

[0027] FIG. **7**G includes a photo representing surface morphology of another sintered target;

[0028] FIG. **7**H includes a photo representing surface morphology of another sintered target;

[0029] FIG. **7**J includes a table representing parameters of the surface morphology photos shown in FIGS. **7**A-**7**H;

[0030] FIG. **8**A includes photos representing hydroxyapatite forming ability of sintered cement. The thermally treated cement produces 10 times more HA during immersion in PBS;

[0031] FIG. **8**B shows a chart representing hydroxyapatite forming ability per surface area of the sintered cement;

[0032] FIG. **8**C shows a chart representing hydroxyapatite forming ability per weight of the sintered cement;

[0033] FIG. **9** includes a flowchart of a PLD process;

[0034] FIG. **10** includes a flowchart of a magnetron spattering process;

[0035] FIG. **11**A includes a photo representing SEM of films deposited on silicon substrate by PLD process at laser energy: (T1)—200 mJ/pulse;

[0036] FIG. **11**B includes a photo representing SEM of a film deposited on silicon substrate by PLD process at laser energy: (T2)—250 mJ/pulse;

[0037] FIG. **11**C includes a photo representing SEM of a film deposited on silicon substrate by PLD process at laser energy: (T3)—300 mJ/pulse;

[0038] FIG. **11**D includes a photo representing SEM of a film deposited on silicon substrate by PLD process at laser energy: (T4)—400 mJ/pulse;

[0039] FIG. **12**A includes a photo showing gutta-percha points;

[0040] FIG. **12**B includes a photo representing an SEM of a film on a gutta-percha point by PLD process;

[0041] FIG. **12**C includes a zoomed-in view of the photo of FIG. **12**B;

[0042] FIG. **12**D includes a zoomed-in view of a different area of the photo shown in FIG. **12**B;

[0043] FIG. **12**E includes a zoomed-in view of a different area of the photo shown in FIG. **12**B;

[0044] FIG. **12**F includes a zoomed-in view of a different area of the photo shown in FIG. **12**B;

[0045] FIG. **13**A includes a photo representing a SEM image of a film on a titanium implant deposited by PLD process;

[0046] FIG. **13**B includes a photo representing a SEM image of a film on another titanium implant deposited by PLD process;

[0047] FIG. **13**C includes a photo representing a SEM image of a film on another titanium implant deposited by PLD process;

[0048] FIG. **13**D includes a photo representing a SEM image of a film on another titanium implant deposited by PLD process;

[0049] FIG. **13**E includes a photo representing a SEM image of a film on another titanium implant deposited by PLD process;

[0050] FIG. **13**F includes a photo representing a SEM image of a film on another titanium implant deposited by PLD process;

[0051] FIG. **13**G includes a table representing the SEM images of the films on the titanium implants deposited by PLD process shown in FIGS. **13**A-**13**F;

[0052] FIG. **14**A includes a chart representing X-Ray analysis confirms amorphous structure of films observed in FIGS. **11**A-**11**C;

[0053] FIG. **14**B includes a chart representing X-Ray analysis, which confirms amorphous structure of films observed in FIGS. **11**A-**11**C;

[0054] FIG. **14**C includes a chart representing Raman analysis, which confirms amorphous structure of films observed in FIGS. **11**A-**110**;

[0055] FIG. **14**D includes a chart representing Raman analysis, which confirms amorphous structure of films observed in FIGS. **11**A-**11**C;

[0056] FIG. **15** includes a chart representing Raman analysis of films deposited on titanium implants using PLD process;

[0057] FIG. **16**A includes a chart representing an EDS elemental analysis of films deposited on titanium implants using PLD process;

[0058] FIG. **166** includes a chart representing an XRF elemental analysis of films deposited on titanium implants using PLD process;

[0059] FIG. **17**A includes a photo of a film for HA-formation study;

[0060] FIG. **17**B includes another photo of a film for the HA-formation study;

[0061] FIG. **17**C includes another photo of a film for the HA-formation study;

[0062] FIG. **17**D includes another photo of a film for the HA-formation study;

[0063] FIG. **17**E includes another photo of a film for the HA-formation study;

[0064] FIG. **17**F includes another photo of a film for the HA-formation study;

[0065] FIG. **17**G includes a chart and table representing a guide for the HA-formation study of the films shown in FIGS. **17**A-**17**F;

[0066] FIG. **18** includes photos representing SEM observation of HA formation on films deposited on gutta-percha;

[0067] FIG. **19** includes photos representing SEM observation of HA formation on films deposited on titanium (the best results highlighted in red boxes);

[0068] FIG. **20**A includes a chart representing XRD analysis of HA formation on MTA coating deposited on gutta-percha;

[0069] FIG. **20**B includes a chart representing XRD analysis of HA formation on MTA coating deposited on gutta-percha;

[0070] FIG. **21**A includes a chart representing Raman analysis of HA formation on MTA coating deposited on titanium;

[0071] FIG. **21**B includes a chart representing Raman analysis of HA formation on MTA coating deposited on titanium;

[0072] FIG. **21**C includes a chart representing Raman analysis of HA formation on MTA coating deposited on titanium;

[0073] FIG. **21**D includes a chart representing Raman analysis of HA formation on MTA coating deposited on titanium;

[0074] FIG. **21**E includes chart representing Raman analysis of HA formation on MTA coating deposited on titanium;

[0075] FIG. **21**F includes a chart representing Raman analysis of HA formation on MTA coating deposited on titanium;

[0076] FIG. **21**G includes a chart representing Raman analysis of HA formation on MTA coating deposited on titanium;

[0077] FIG. **22**A includes a photo representing EDS spectra of HA formed on MTA coating deposited on gutta-percha shown in FIG. **22**A after 21 day of immersion in SBF;

[0078] FIG. **22**B includes a chart representing EDS spectra of HA formed on MTA coating deposited on gutta-percha after 21 day of immersion in SBF;

[0079] FIG. **23**A includes a photo representing an EDS map of HA formed on MTA coating deposited on titanium after 21 day of immersion in SBF;

[0080] FIG. **23**B includes a photo representing Ca-Ka portion of the EDS map of HA formed on MTA coating deposited on titanium after 21 day of immersion in SBF;

[0081] FIG. **23**C includes a photo representing P-Ka portion of the EDS map of HA formed on MTA coating deposited on titanium after 21 day of immersion in SBF;

[0082] FIG. **23**D includes a photo representing O-Ka portion of the EDS map of HA formed on MTA coating deposited on titanium after 21 day of immersion in SBF;

[0083] FIG. **23**E includes a photo representing Si-Ka portion of the EDS map of HA formed on MTA coating deposited on titanium after 21 day of immersion in SBF;

[0084] FIG. **23**F includes a photo representing S-Ka portion of the EDS map of HA formed on MTA coating deposited on titanium after 21 day of immersion in SBF;

[0085] FIG. **23**G includes a photo representing Ti-Ka portion of the EDS map of HA formed on MTA coating deposited on titanium after 21 day of immersion in SBF;

[0086] FIG. **23**H includes a photos representing Na-Ka portion of the EDS map of HA formed on MTA coating deposited on titanium after 21 day of immersion in SBF;

[0087] FIG. **23**I includes a photo representing CI-Ka portion of the EDS map of HA formed on MTA coating deposited on titanium after 21 day of immersion in SBF;

[0088] FIG. **24**A includes a photo representing an HA study at day 1;

[0089] FIG. **24**B includes another photo representing the HA study at day 1;

[0090] FIG. **24**C includes another photo representing the HA study at day 1;
[0091] FIG. **24**D includes another photo representing the HA study at day 1;
[0092] FIG. **24**E includes another photo representing the HA study at day 1
[0093] FIG. **24**F includes another photo representing the HA study at day 1;
[0094] FIG. **24**G includes another photo representing the HA study at day 1;
[0095] FIG. **25**A includes a photo representing an HA study at day 3;
[0096] FIG. **25**B includes another photo representing the HA study at day 3;
[0097] FIG. **25**C includes another photo representing the HA study at day 3;
[0098] FIG. **25**D includes another photo representing the HA study at day 3;
[0099] FIG. **25**E includes another photo representing the HA study at day 3;
[0100] FIG. **25**F includes another photo representing the HA study at day 3;
[0101] FIG. **25**G includes another photo representing the HA study at day 3;
[0102] FIG. **26**A includes a photo representing an HA study at day 7;
[0103] FIG. **26**B includes another photo representing the HA study at day 7;
[0104] FIG. **26**C includes another photo representing the HA study at day 7;
[0105] FIG. **26**D includes another photo representing the HA study at day 7;
[0106] FIG. **26**E includes another photo representing the HA study at day 7;
[0107] FIG. **26**F includes another photo representing the HA study at day 7;
[0108] FIG. **26**G includes another photo representing the HA study at day 7;
[0109] FIG. **27**A includes a photo representing an HA study at day 14;
[0110] FIG. **27**B includes another photo representing the HA study at day 14;
[0111] FIG. **27**C includes another photo representing the HA study at day 14;
[0112] FIG. **27**D includes another photo representing the HA study at day 14;
[0113] FIG. **27**E includes another photo representing the HA study at day 14;
[0114] FIG. **27**F includes another photo representing the HA study at day 14;
[0115] FIG. **27**G includes another photo representing the HA study at day 14;
[0116] FIG. **28**A includes a photo representing an HA study at day 21;
[0117] FIG. **28**B includes another photo representing the HA study at day 21;
[0118] FIG. **28**C includes another photo representing the HA study at day 21;
[0119] FIG. **28**D includes another photo representing the HA study at day 21;
[0120] FIG. **28**E includes another photo representing the HA study at day 21;
[0121] FIG. **28**F includes another photo representing the HA study at day 21;
[0122] FIG. **29**A includes a photo representing an HA study at day 28;
[0123] FIG. **29**B includes another photo representing the HA study at day 28;
[0124] FIG. **29**C includes another photo representing the HA study at day 28;
[0125] FIG. **29**D includes another photo representing the HA study at day 28;
[0126] FIG. **29**E includes another photo representing the HA study at day 28;
[0127] FIG. **29**F includes another photo representing the HA study at day 28;
[0128] FIG. **29**G includes another photo representing the HA study at day 28;
[0129] FIG. **29**H includes another photo representing the HA study at day 28;
[0130] FIG. **30**A includes a chart representing EDS results of HA formation study;
[0131] FIG. **30**B includes another chart representing EDS results of the HA formation study;
[0132] FIG. **30**C includes another chart representing EDS results of the HA formation study;
[0133] FIG. **30**D includes another chart representing EDS results of the HA formation study;
[0134] FIG. **30**E includes another chart representing EDS results of the HA formation study;
[0135] FIG. **30**F includes another chart representing EDS results of the HA formation study;
[0136] FIG. **31**A includes a photo representing an EDS map (film before immersion, PTi-5);
[0137] FIG. **31**B includes a photo representing a Ti-Ka EDS map (film before immersion, PTi-5);
[0138] FIG. **31**C includes a photo representing a Ca-KA EDS map (film before immersion, PTi-5);
[0139] FIG. **31**D includes a photo representing a Si—K EDS map (film before immersion, PTi-5);
[0140] FIG. **31**E includes a photo representing a Al—K EDS map (film before immersion, PTi-5);
[0141] FIG. **31**F includes a photo representing a S-KA EDS map (film before immersion, PTi-5);
[0142] FIG. **31**G includes a photo representing a **0**-KA EDS map (film before immersion, PTi-5);
[0143] FIG. **31**H includes a photo representing a Mg—K EDS map (film before immersion, PTi-5);
[0144] FIG. **31**I includes a photo representing a P-Ka EDS map (film before immersion, PTi-5);
[0145] FIG. **31**J includes a chart representing the EDS maps shown in FIGS. **31**A-**31**I;
[0146] FIG. **32**A includes a photo representing an EDS map (3 days immersion, PTi-5);
[0147] FIG. **32**B includes a photo representing a Ti-Ka EDS map (3 days immersion, PTi-5);
[0148] FIG. **32**C includes a photo representing a Ca-KA EDS map (3 days immersion, PTi-5);
[0149] FIG. **32**D includes a photo representing a P-KA EDS map (3 days immersion, PTi-5);
[0150] FIG. **32**E includes a photo representing a CI-KA EDS map (3 days immersion, PTi-5);
[0151] FIG. **32**F includes a photo representing a S-KA EDS map (3 days immersion, PTi-5);
[0152] FIG. **32**G includes a photo representing a **0**-KA EDS map (3 days immersion, PTi-5);
[0153] FIG. **32**H includes a photo representing a Mg—K EDS map (3 days immersion, PTi-5);

[0154] FIG. **32**I includes a photo representing a Na-Ka EDS map (3 days immersion, PTi-5); and

[0155] FIG. **32**J includes a chart representing the EDS maps shown in FIGS. **32**A-**32**I.

SUMMARY OF THE INVENTION

[0156] A dense MTA tile is produced through a series of process steps which creates a Target suitable for physical vapor deposition (PVD). The resulting MTA material has improved biological effects and produces HA at an accelerated rate when in the presence of simulated body fluid. The resulting Target can then be micronized or used to deposit a thin layer as desired, such as upon an obturation point. Conventional obturation points such as those made of gutta percha materials are useful in the application of the present invention.

[0157] According to one embodiment of the invention, a deposited thin layer of a cured or uncured MTA (Mineral Trioxide Aggregate) is deposited on the surface of otherwise conventional gutta-percha points. The material produces hydroxyl apatite (HA) mineral in the presence of Phosphate Buffered Saline which is beneficial in the formation of cementum like material for natural sealing of dental root canals.

[0158] In another embodiment cured MTA is deposited onto Gutta-percha points using a PVD method.

[0159] Another embodiment comprises the use of uncured MTA molded onto the surface of a gutta-percha point using a compression molding technique.

[0160] Still another inventive embodiment comprises the use of cured MTA compressed onto the surface of the gutta-percha using a compression molding technique.

[0161] A further embodiment of the invention includes the use of cured MTA molded onto the surface of the gutta-percha using an injection molding technique.

[0162] A still further embodiment comprises the use of uncured MTA molded onto the surface of the gutta-percha using an injection molding technique.

[0163] Another preferred embodiment is placing cured MTA onto implantable and prosthetic devices using PVD method

DETAILED DESCRIPTION OF THE INVENTION

[0164] A dense MTA with improved biological effects is produced through special processing techniques. The resulting dense MTA material has improved biological effects and in the presence of simulated body fluid and produces HA at an increased and accelerated rate.

[0165] Dense MTA targets can be created for use in physical vapor deposition (PVD) to provide a thin layer of MTA on the surface of implantable devices such as dental implants, endodontic obturation materials and the like. PVD techniques include:

[0166] Cathodic Arc Deposition: In which a high-power electric arc discharged at the target (source) material blasts away some into highly ionized vapor to be deposited onto the work piece.

[0167] Electron beam physical vapor deposition: In which the material to be deposited is heated to a high vapor pressure by electron bombardment in "high" vacuum and is transported by diffusion to be deposited by condensation on the (cooler) work piece.

[0168] Evaporative deposition: In which the material to be deposited is heated to a high vapor pressure by electrically resistive heating in "low" vacuum.

[0169] Pulsed laser deposition: In which a high-power laser ablates material from the target into a vapor.

[0170] Sputter deposition: In which a glow plasma discharge (usually localized around the "target" by a magnet) bombards the material sputtering some away as a vapor for subsequent deposition.

[0171] A thin layer of cured MTA (Mineral Trioxide Aggregate) is deposited on the surface of an implantable device.

[0172] The improved MTA is particularly suitable for obturating and sealing dental root canals. The improved MTA provides a stable barrier to bacterial and fluid leakage in the root canal. The accelerated generation of HA will also help promote the growth of new bone and tissue surrounding the root tip area. The improved MTA should also provide a stable barrier to bacteria and fluid leakage in the root canal system of the tooth.

[0173] The dense MTA material, Targets, may also be ground into small particles for use in Dental products or as a MTA powder with improved biological effects.

Target Creation Process

[0174] A method for forming the dense MTA material (Target) may include one or more of the steps/processes described below and further shown in FIG. **1**

Mixing Process

[0175] Mixing (white) Portland Cement (WPC or PC) to Deionized water having a ratio in the range of about 10:1 to about 1:10, preferably about 5:1 to about 1:5, and more preferably about 5:1 to about 1:1 (e.g., about 3:1 such as about 3 parts PC (WPC) to about 1 part deionized water). The mixture is thoroughly blended and vacuum is drawn out to create a harmonized cake mix and then placed in molds.

Curing Process

[0176] Once the mixed cement is put in molds, the molds are placed in a humidity chamber to cure. The humidity chamber is set at 36° C. with 90% Relative Humidity (RH) from about 5 hours to about 10 days, and preferably from about 12 hours to about 5 days (e.g., about 2 days).

Post Cure Baking Process

[0177] Once the cement is cured, the set cement is placed in a Post cure bake oven set at a temperature from about 50° C. to about 500° C., and preferably from about 100° C. to about 250° C. (e.g., about 160° C.) for a time ranging from about 15 mins to about 2 days, and preferably from about 1 hour to about 12 hours (e.g., about 6 hours).

Ball Milling and Micronizing Process

[0178] The target creation process may include a micronizing step. Once the cement is post baked, it is then pulverized, micronized and sieved to a particle size ranging from about 1 micron to about 200 microns, and preferably from about 10 microns to about 100 microns (e.g., about 53 microns (μ53)).

Sintering Process

[0179] The target creation process may include a Sintering Step. The Powder Micronized MTA is pressed into a target then placed into a sintering chamber for a first heat treatment at a temperature ranging from about 25° C. to about 400° C., preferably from about 50° C. to about 250 degrees Celsius (e.g., about 125° C.) for a time period of about 5 mins to about 5 hours, preferably from about 15 mins to about 2 hours (e.g., about 30 to about 40 mins) at little or substantially no pressure. Optionally, the sintering process may include a second heat treatment, though not required. When included, the temperature may be increased to a third heat treatment temperature that is higher than the first heat treatment temperature, the second heat treatment temperature ranging from about 275° C. to about 650° C., and preferably from about 350° C. to about 525° C. (e.g., about 450° C.) for a time period ranging from about 5 minutes to about 12 hours, and preferably from about 15 mins to about 5 hours (e.g., about 1 to 2 hours) at a pressure ranging from about 5000 pounds/in^2 (psi) to about 50,000 psi, and preferably from about 10,000 psi to about 25,000 psi (e.g., about 15,000 psi). Optionally, the sintering process may include a third heat treatment, though not required. When included, the heat treatment temperature of the sintering process may be increased to a third heat treatment temperature that is higher than the second heat treatment temperature, the third heat treatment temperature ranging from about 550° C. to about 1100° C., and preferably from about 650° C. to about 975° C. (e.g., about 750° C. to 850° C.) for a period of time ranging from about 30 mins to about 2 days, and preferably from about 2 hours to about 1 day (e.g., about 4 hours to about 12 hours) at a pressure ranging from about 1,000 psi to about 50,000 psi, and preferably from about 7,500 psi to about 35,000 psi (e.g., about 15,000 psi to 20,000 psi).

HIP Process

[0180] The target creation process may include a hot isostatic pressing (HIP) step/process. The set sintered targets may be placed into a HIP chamber at a temperature ranging from about 250° C. to about 1500° C., and preferably from about 500° C. to about 1000° C. (e.g., about 750° C. to about 850° C.) for a period of time ranging from about 30 mins to about 2 days, and preferably from about 2 hours to about 1 day (e.g., about 4 hours to about 12 hours) at a pressure ranging from about 1,000 psi to about 50,000 psi, and preferably from about 7,500 psi to about 35,000 psi (e.g., about 15,000 psi to 20,000 psi).

Post HIP, NGMTA Improved Biological Effect MTA

[0181] The HIPped targets may be micronized to a particle size ranging from about 1 micron to about 200 microns, and preferably from about 10 microns to about 100 microns (e.g., about 53 microns (μ53)) wherein the resultant powder MTA has improved biological effects and produces HA at an accelerated rate.

Ranges of Parameters

[0182] The experimented parameters for one or more of the above steps and/or processes may range from:

[0183] The temperature(s) may range from about 25° C. to about 1500° C., preferably from about 500° C. to about 1200° C.

[0184] The pressure(s) may range from about 0 psi to about 50,000 psi, preferably from about 15,000 psi to about 20,000 psi.

[0185] The time periods may range from about 5 mins to about 10 days, preferably from about 2 hours to about 5 hours.

[0186] The preferred method of coating medical devices with MTA is physical vapor deposition (PVD), using magnetron sputtering. Alternative methods of Physical Vapor Deposition may also include Pulsed Laser Deposition (PLD), Magnetron Sputtering, and the like as above discussed

[0187] Other useful techniques for coating medical devices with MTA include:

[0188] Compression molding which entails sprinkling MTA on the substrate during compression molding process; and,

[0189] Micronized powder and spraying, this entails blasting the substrate with high velocity spray of MTA.

[0190] In one example of the invention, optimum parameters for a dense target producing increased HA generation (FIG. **8**) include a heat treatment profile having a first heat treatment of about 120° C. at about 0 psi for about 1 hour, a second heat treatment of about 450° C. at about 15,000 psi for about 2 hours, and a third heat treatment of about 850° C. at about 20,000 psi for about 4 hours (FIGS. **2-7**).

Pulsed Laser Deposition (PLD)

[0191] This is a thin film deposition technique where a high-power pulsed laser beam is focused inside a vacuum chamber to strike a target of the material that is to be deposited. This material is vaporized from the target (in a plasma plume) which deposits it as a thin film on the substrate (in this case the GP points); this process occurs in ultra-high vacuum.

[0192] While the basic-setup is simple relative to many other deposition techniques, the physical phenomena of laser-target interaction and film growth are quite complex. When the laser pulse is absorbed by the target, energy is first converted to electronic excitation and then into thermal, chemical and mechanical energy resulting in evaporation, ablation, plasma formation and even exfoliation. The ejected species expand into the surrounding vacuum in the form of a plume containing many energetic species including atoms, molecules, electrons, ions, clusters, particulates and molten globules, before depositing on the substrate.

Magnetron Sputtering

[0193] High Power Impulse Magnetron Sputtering (HIPIMS or HiPIMS, also known as high-power pulsed magnetron sputtering, HPPMS) is a method for physical vapor deposition of thin films which is based on magnetron sputter deposition. HIPIMS utilizes extremely high power densities of the order of kW·cm^{-2} in short pulses (impulses) of tens of microseconds at low duty cycle (on/off time ratio) of <10%.

[0194] Distinguishing features of HIPIMS are a high degree of ionisation of the sputtered material and a high rate of molecular gas dissociation which result in high density of deposited films. The ionization and dissociation degree increase according to the peak cathode power. The limit is determined by the transition of the discharge from glow to arc phase. The peak power and the duty cycle are selected so

as to maintain an average cathode power similar to conventional sputtering (1-10 $W \cdot cm^{-2}$).

[0195] By using magnets behind the cathode to trap the free electrons in a magnetic field directly above the target surface, these electrons are not free to bombard the substrate to the same extent as with diode sputtering. At the same time the extensive, circuitous path carved by these same electrons when trapped in the magnetic field, enhances their probability of ionizing a neutral gas molecule by several orders of magnitude. This increase in available ions significantly increases the rate at which target material is eroded and subsequently deposited onto the substrate.

[0196] MTA films were deposited on Silicone, Gutta Percha and Titanium samples using PVD. The thickness and concentration can be altered based on duration and power levels (FIGS. **11-13**). Characterization of raw material sintering of targets for Pulsed Laser Deposition (PLD) and deposition of material in the form of thin films on testing substrates, gutta-percha and titanium implants (FIGS. **13-16**). To ensure that physical vapor deposition (PVD) does not change chemical composition of raw materials, the full materials characterization of WPC (White Portland Cement) included elemental analysis by electron dispersive spectroscopy (EDS, FIG. **16**), phase analysis by X-ray diffractometry (XRD, FIG. **14**), composition analysis using (micro-Raman, FIGS. **14**, **15**), density measurements and morphological studies by scanning electron microscopy (SEM, FIGS. **11-13**).

Deposition of Films on Alternate Materials

[0197] PVD can also be used to deposit a thin layer of MTA on a variety of surfaces. Feasibility has been established for PVD of MTA on polyisoprene and ceramic surfaces. Other potential applications include deposition of a MTA film on variety of metal or ceramic surfaces such as NiTi, Titanium, stainless steel, and porcelain.

[0198] From HIP-Sintered WPC targets supplied Pulsed Laser Deposition PLD was performed and uniformity of thickness and composition of deposited material was studied on Implantable and prosthetic devices.

HA (Hydroxyapatite) Formation Study

[0199] In order to confirm bio-activity of MTA coating the HA-forming ability was tested on films deposited on silicon, gutta-percha and titanium. The deposited films were soaked in simulated body fluids (SBF) at 37° C. for 1, 3, 7, 14 and 21 days. The HA formation was observed after 1 day, whereas typically HA formation is not first observed until 7 days. (FIG. **17**).

[0200] The formation of hydroxyl apatite (HA) and other phosphates were confirmed by SEM imaging (FIGS. **18**, **19**) and analyzed by XRD and micro-Raman (FIGS. **20**, **21**A-**21**B). The Ca/P ratio of produced HA was studied by EDS and newly acquired x-ray fluorescence (XRF) (FIGS. **22**, **23**).

[0201] Thus, it should be evident that the invention as disclosed herein carries out one or more of the objects of the present invention set forth above and otherwise constitutes an advantageous contribution to the art. As will be apparent to persons skilled in the art, modifications can be made to the preferred embodiments disclosed herein without departing from the spirit of the invention, the scope of the invention herein being limited solely by the scope of the attached claims.

What is claimed is:

1. An implantable dental device comprising a layer of mineral trioxide aggregate that produces hydroxyl apatite in the presence of phosphate buffered saline.

2. An implantable dental device as in claim **1** wherein said device is an obturation point.

3. An implantable device as in claim **1** wherein said obturation point comprises gutta-percha.

4. A method for producing hydroxyl apatite on a dental device comprising the step of preparing a tile of mineral trioxide aggregate.

5. A method as in claim **4** further comprising forming a mixture by mixing Portland cement and deionized water in an amount of from about 10:1 to about 1:10.

6. A method as in claim **5** wherein said mixture is placed into a mold and cured in a humidity chamber.

7. A method as in claim **6** wherein said humidity chamber is set at 36 degrees Celsius with about a 90 percent relative humidity for from about 5 hours to about 10 days.

8. A method as in claim **7** wherein said cured mixture is subjected to a second heating by heating to from about 50 to about 500 degrees Celsius for from about 15 minutes to about 2 days.

9. A method as in claim **8** wherein said method includes micronizing said cured tile.

10. A method as in claim **9** wherein said micronizing includes ball-mill grinding said tile to a particle size of from about 1 to about 200 microns.

11. A method as in claim **10** wherein said micronizing includes ball-mill grinding said tile to a particle size of from about 10 to about 100 microns.

12. A method as in claim **11** wherein said micronizing includes ball-mill grinding said tile to a particle size of about 53 microns.

13. A method as in claim **9** wherein said micronized tile is sintered at a temperature of from about 25 to about 400 degrees Celsius for a period of from about 5 minutes to about 5 hours.

14. A method as in claim **13** wherein said sintered, micronized tile is subjected to a second sintering temperature of from about 275 to about 650 degrees Celsius for from about 5 minutes to about 12 hours.

15. A method as in claim **14** wherein said second sintering step is conducted at a pressure of from about 5000 psi to about 50,000 psi.

16. A method as in claim **14** wherein said sintered, micronized tile is subjected to a third sintering temperature of from about 550 to about 1100 degrees Celsius for from about 30 minutes to about 2 days.

17. A method as in claim **16** wherein said third sintering step is conducted at a pressure of from about 1000 psi to about 50,000 psi.

18. A method as in claim **9** wherein said step of depositing includes physical vapor deposition of said micronized tile.

19. A method as in claim **9** wherein said step of depositing includes hot isostatic pressing of said micronized tile.

20. A method as in claim **9** wherein said step of depositing includes hot isostatic pressing of said micronized tile.

21. A method as in claim **9** wherein said step of depositing includes molding of said micronized tile.

* * * * *